Journal of Controlled Release 334 (2021) 37–51

Contents lists available at ScienceDirect

Journal of Controlled Release

journal homepage: www.elsevier.com/locate/jconrel

Relating transdermal delivery plasma pharmacokinetics with *in vitro* permeation test (IVPT) findings using diffusion and compartment-in-series models

Xin Liu [a], Yuri G. Anissimov [b], Jeffrey E. Grice [a,*], Hanumanth Srikanth Cheruvu [a], Priyanka Ghosh [c], Sam G. Raney [c], Howard I. Maibach [d], Michael S. Roberts [a,e]

[a] *Therapeutics Research Group, The University of Queensland Diamantina Institute, The University of Queensland, Woolloongabba, QLD 4102, Australia*
[b] *School of Environment and Science, Griffith University, Parklands Drive, Southport, QLD 4222, Australia*
[c] *Division of Therapeutic Performance, Office of Research and Standards, Office of Generic Drugs, U.S. Food and Drug Administration, Silver Spring, MD, USA*
[d] *Department of Dermatology, University of California, San Francisco, California, USA*
[e] *Therapeutics Research Centre, University of South Australia Division of Clinical and Health Sciences, Basil Hetzel Institute for Translational Medical Research, The Queen Elizabeth Hospital, Woodville, SA 5011, Australia*

ARTICLE INFO

Keywords:
in vitro skin permeation tests (*IVPT*)
in vivo topical absorption
Transdermal
Plasma concentration
Diffusion models
Compartment-in-series skin models
in vitro – in vivo relationship (IVIVR), pharmacokinetics

ABSTRACT

Increasing emphasis is being placed on using *in vitro* permeation test (*IVPT*) results for topical products as a surrogate for their *in vivo* behaviour. This study sought to relate *in vivo* plasma concentration – time pharmacokinetic (PK) profiles after topical application of drug products to *IVPT* findings with mechanistic diffusion and compartment models that are now widely used to describe permeation of solutes across the main skin transport barrier, the stratum corneum. Novel *in vivo* forms of the diffusion and compartment-in-series models were developed by combining their *IVPT* model forms with appropriate *in vivo* disposition functions. Available *in vivo* and *IVPT* data were then used with the models in data analyses, including the estimation of prediction intervals for *in vivo* plasma concentrations derived from *IVPT* data. The resulting predicted *in vivo* plasma concentration - time profiles for the full models corresponded closely with the observed results for both nitroglycerin and rivastigmine at all times. In contrast, reduced forms of these *in vivo* models led to discrepancies between model predictions and observed results at early times. A two-stage deconvolution procedure was also used to estimate the *in vivo* cumulative amount absorbed and shown to be linearly related to that from *IVPT*, with an acceptable prediction error. External predictability was also shown using a separate set of *in vitro* and *in vivo* data for

Abbreviations: ˆ.. (s), notation showing parameter expressed in Laplace transform; *%PE*, the percentage prediction error; A, surface area of application; AIC, Akaike Information Criterion; $AUC_{0\text{-}last}$, area under plasma concentration-time curve for the sampling period; $AUC_{0\text{-}\infty}$, area under plasma concentration-time curve extrapolated to infinity; AUC_{ss}, area under plasma concentration-time curve at steady state on multiple dosing; *B*, relative permeability of the SC to the VE; BA, bioavailability; BE, bioequivalence; *CL*, plasma clearance; *C(t)*, plasma concentration of solute; C_m, solute concentration in the membrane; $C_{max,ss}$, maximum plasma concentrations seen at steady state on multiple dosing; cosh*()*, hyperbolic cosine function; C_v, solute concentration in the donor (product); De, dermis; D_m, solute diffusion coefficient in the membrane; *e()*, exponential function; *EPI*, epidermis (*i.e.* SC + VE) (also as $_{epi}$ in subscript form); *ER*, extended release; *G*, ratio of the SC to VE diffusion times; h_m, membrane thickness; *IVIVC*, *in vitro - in vivo* correlation; *IVIVR*, *in vitro – in vivo* relationship; *IVPT*, *in vitro* permeation test; J_{ss}, steady state flux; *k*, diffusion rate constant; k_{el}, elimination rate constant; k_{10}, elimination rate constant for a multicompartment disposition model (= k_{el} for a one compartment model); k_{12}, k_{21}, inter-compartment rate constants for a 2-compartment disposition model; k_{13}, k_{31}, inter-compartment rate constants for the third compartment in a 3-compartment disposition model; K_{sc}, partition coefficient between the SC and donor (product); $K_{ve\text{-}sc}$, partition coefficient between the SC and VE; *lag*, lag time (*e.g.* lag_{sc} and lag_{epi}); *linear*, in subscript form indicates a linear (steady state) portion of a curve; PK, pharmacokinetic; *Q(t)*, cumulative amount permeated through skin; R_0, constant input rate from donor (product) to the skin; *s*, Laplace operator; SC, stratum corneum (also as $_{sc}$ in subscript form); SC_1, amount of solute in SC compartment 1; SC_2, amount of solute in SC compartment 2; SC_3, amount of solute in SC compartment 3; *sinh()*, hyperbolic sine function; *t*, time; t_d, diffusion time; TDS, transdermal delivery system; V_d, volume of distribution of plasma compartment; VE, viable epidermis (also as $_{ve}$ in subscript form); WLS, weighted least squares; X_c, amount of solute in the central compartment; X_{p1}, amounts of solute in the peripheral compartment 1; X_{p2}, amounts of solute in the peripheral compartment 2.

* Corresponding author at: Therapeutics Research Group, The University of Queensland Diamantina Institute, Level 5, Translational Research Institute, 37 Kent Street, Woolloongabba, QLD 4102, Australia.
E-mail address: jeff.grice@uq.edu.au (J.E. Grice).

https://doi.org/10.1016/j.jconrel.2021.04.010
Received 23 October 2020; Received in revised form 8 April 2021; Accepted 11 April 2021
Available online 20 April 2021

different nitroglycerin patches. This work suggests that mechanistic and physiologically based pharmacokinetic models can be used to predict *in vivo* behaviour from *IVPT* data for topical products.

1. Introduction

Products applied to the skin may be used to deliver drugs into and/or through the skin for local and/or systemic action for a variety of disease indications. These products can be categorized according to the intended site of action. When drug products are applied to the skin for local cutaneous action, they are designated as topical drug products and are most commonly available as semisolid dosage forms such as gels, creams or ointments. On the other hand, when drug products are applied to the skin for systemic action, they are classified as transdermal drug products and are most commonly available as transdermal delivery systems (TDS; also known as transdermal patches) [1]. Despite these differences in the intended site of action, the fundamental mechanisms of drug diffusion through the skin are essentially the same in all cases, irrespective of whether the intended site of action is local for a topical product or systemic for a transdermal product. For the purposes of developing pharmacokinetic models, it is therefore possible to begin with modelling the diffusion of drugs from transdermal products for which pharmacokinetic (PK) data is available for comparison, and with which the drug delivery from TDS dosage forms may be relatively less complex to model.

Analysing PK data of a drug can be one of the most accurate, sensitive and reproducible ways to evaluate bioavailability (BA) and bioequivalence (BE) between two or more formulations. The cutaneous and/or systemic PK of topical and transdermal products can be evaluated experimentally using various approaches, including *in vivo* dermatopharmacokinetic analysis of stratum corneum (SC) concentration depth profiles [2–4], dermal microdialysis [5], dermal microperfusion [6], and drug concentrations quantified in blood/plasma/serum [7] or urine [8–12]. Among these approaches, plasma or serum drug levels are the most readily available data, while it is technically more challenging to monitor drug local concentration in SC or dermis.

An alternative approach to investigating cutaneous or systemic PK for topically applied drugs is to predict *in vivo* PK based on *in vitro* permeation test (*IVPT*) results, using *in vitro-in vivo* relationship (*IVIVR*) models. These pharmacokinetic models are particularly useful in situations where reliable *in vivo* information about the local cutaneous PK of a topical drug is not easy to obtain, or when the systemic PK of a transdermal drug cannot be studied easily or safely. For example, it may not be feasible to measure the local tissue concentrations of diclofenac or lidocaine experimentally after topical administration of a diclofenac or lidocaine topical delivery system indicated for the relief of pain. To predict systemic or cutaneous PK profiles for such products, it is practical to begin with a model that convolutes *IVPT* data (the input function) with an *in vivo* drug disposition profile. *IVPT* data can be generated experimentally and the *in vivo* data are available in the literature for some drugs, which can serve as model drugs to develop and validate the model by comparing predicted PK profiles with experimentally observed data.

Pharmacokinetic modelling of dermal drug delivery from topical and transdermal products requires an understanding of both the physiology of the skin, the physicochemical properties of the drug, and the attributes of the products. Variations in drug transport may be observed among different topical and/or transdermal drug products due to the interaction of inactive ingredients with the skin and/or with the drug molecule. However, once the drug molecule is released from the dosage form, the underlying transport mechanism across the skin is essentially the same, regardless of whether the drug molecule is indicated for local (topical) or systemic (transdermal) action, and regardless of the dosage form.

An important practical consideration for the development of pharmacokinetic models for semisolid dosage forms like gels and creams is that they can undergo metamorphosis during dose dispensing and application, due to evaporation/drying of the aqueous or alcoholic phases in the dosage form. Also, these products are typically applied to the skin as a thin film (a finite dose) in which the amount of soluble drug dynamically changes (decreases) due to depletion as the drug partitions into the skin, and due to changes in solubility as the volatile components of the dosage form evaporate. Consequently, modelling the release of the drug from a finite dose of such dosage forms requires an understanding of the exceptionally complex and potentially variable metamorphosis that can occur, and the resulting non-steady state drug delivery. In contrast, TDS products are less complex to model because they contain a "pseudo-infinite" drug load to help maintain a relatively constant drug delivery rate over the entire period of application, and the dosage form is relatively stable and consistent because metamorphosis is minimal. Therefore, a time-dependent release rate can be calculated more reliably for these products. Given the relative lack of model complexity with TDS compared to semisolid dosage forms, and since *in vivo* plasma or serum PK data for TDS products are available and can be used to evaluate the predictions of different pharmacokinetic models, two drugs delivered by TDS, nitroglycerin and rivastigmine, were selected for model evaluation in this work.

The authors [13–16] and others [17–24] have developed various diffusion based pharmacokinetic models to describe skin permeation, primarily with data obtained from *IVPT* studies. However, some of these models may be too computationally complex to be practically useful in describing the processes involved. Simple compartmental models have been used as alternatives to diffusion models in percutaneous absorption [25,26]. Many researchers represent the skin as a single well-stirred compartment to simplify the mathematics and this type of compartment model gives acceptable results for solutes that have a short diffusion time. We have recently developed a more general, *n*-compartment-in-series model as an approximation of the diffusion model [27]. The use of compartment-in-series models as alternative representations of skin transport is illustrated in Fig. 1.

The authors have previously derived diffusion equations for the cumulative amount of solute permeating through SC from a constant donor (product) concentration into a sink receptor [13]. Here, we extend that work to consider both the SC and the full epidermis, *i.e.* SC with viable epidermis as the skin barrier. These diffusion equations were solved by using analytical Laplace solutions. An infinite dose provided by a TDS system that provides a constant donor (product) concentration was chosen in this work as this, combined with sink receptor conditions, can be used in *IVPT* studies to achieve a linear steady-state skin flux. These relatively less complex conditions are reasonably representative of the pseudo-infinite, relatively constant dose that can be delivered with transdermal products, and of the practically infinite sink produced *in vivo* by the highly efficient clearance of drug from the skin to the systemic circulation. The use of an infinite dose was advantageous, as it allowed us to develop and verify the skin transport parameters of a dermal model, without the additional complexity of a finite dose of a semisolid dosage form undergoing variable metamorphoses. The expectation was that additional complexity could be added to the model once the fundamental skin transport parameters were well described. In this paper, we explore the use of reduced forms of the full diffusion model, compartment-in-series models as an approximation of the full diffusion model and reduced forms of the compartment-in-series model, as alternatives to the full diffusion models as these simplify the mathematics (Fig. 2). To compare the predicted *in vivo* absorption of solutes applied to the skin with the observed plasma concentrations after topical application, we tested appropriate pharmacokinetic models of *in vivo*

diffusion and the alternative approximation and compartment models. We then used simulations, *IVPT* experiments, nonlinear regression and numerical deconvolution of *in vivo* data to verify the suitability of our models for describing *in vivo* plasma concentrations. *In vitro - in vivo* relationships (*IVIVR*) for TDS were explored using one stage convolution and two stage deconvolution approaches.

2. Methods

2.1. Models used to predict in vivo plasma pharmacokinetics after topical application

Fig. 2 shows a schematic representation of four models describing drug transport through skin that were considered in this work. We describe the solutions for both *in vitro* and *in vivo* applications using the following four approaches: 1) the "full" unsteady diffusion model (Model A); 2) a "reduced" steady-state skin flux diffusion model (Model B); 3) the "full" compartment-in-series model considering forward and backward transport processes (Model C); 4) a "simplified" compartment-in-series model considering forward only transport processes (Model D) and a reduced compartment-in-series, which we found was identical to Model B. In general, the models were derived in the Laplace domain as a convolution of skin permeation function (diffusion or compartment-in-series model) with body disposition functions.

2.1.1. "Full" unsteady diffusion models (Model A)

Two unsteady diffusion models are used to describe the transport of solutes through human skin studied in an *IVPT* system. The first model (Model A(i)), in which the SC is assumed to be a single-layer barrier for solute permeation through the skin, is referred to as the unsteady SC *IVPT* diffusion model. In this model, diffusion through the SC is defined by the diffusion equation shown in Fig. 2, with an initial condition $C_{sc}(x,0) = 0$ and boundary conditions $C_{sc}(0,t) = K_{sc}C_v$ and $C_{sc}(h_{sc},t) = 0$, where $C_{sc}(x,t)$ is solute concentration at distance x and time t in the SC of thickness h_{sc}, K_{sc} is partition coefficient between SC and donor (product) and C_v is donor solute concentration. Together, with the Laplace variable s, these yield the Laplace domain solution $\widehat{Q}_{sc}(s)$, for the cumulative amount permeating through SC ($Q_{sc}(t)$) *versus* time (t): [13]:

$$\widehat{Q}_{sc}(s) = \frac{J_{ss,sc}A}{s^2}\frac{\sqrt{st_{d,sc}}}{sinh\sqrt{st_{d,sc}}} \tag{1}$$

where A is the surface area of application, $t_{d,sc}$ is the SC diffusion time and $J_{ss,sc}$ is the SC steady-state flux.

The corresponding expression for the SC permeation flux ($J_{sc}(t)$) in the Laplace domain, $\widehat{J}_{sc}(s)$, is given by:

$$\widehat{J}_{sc}(s) = \frac{J_{ss,sc}}{s}\frac{\sqrt{st_{d,sc}}}{sinh\sqrt{st_{d,sc}}} \tag{2}$$

In the second model (Model A(ii)), which is referred to as the unsteady epidermal IVPT diffusion model, the SC and the viable epidermis (VE) are assumed to form a two-layer barrier for solute permeation through the skin [13,28]. In this Model (A(ii)), diffusion through the SC and VE are defined by the diffusion equations shown in Fig. 2, with initial conditions of $C_{sc}(x,0) = C_{ve}(x,0) = 0$ and boundary conditions $C_{sc}(0,t) = K_{sc}C_v$, $C_{ve}(h_{ve},t) = 0$, $C_{ve}(0,t) = K_{ve-sc}C_{sc}(h_{sc},t)$ and a continuity of flux across the SC-VE interface, where $C_{ve}(x,t)$ is solute concentration at distance x and time t in viable epidermis of thickness h_{ve} and $K_{ve\text{-}sc}$ is partition coefficient between VE and SC. The Laplace domain solution for the cumulative amount permeating through epidermis ($Q_{epi}(t)$) is:

$$\widehat{Q}_{epi}(s) = \frac{J_{ss,sc}A\sqrt{st_{d,sc}}}{s^2\left(B\frac{\sqrt{st_{d,sc}}}{\sqrt{st_{d,sc}/G}}cosh\sqrt{st_{d,sc}}sinh\sqrt{st_{d,sc}/G} + sinh\sqrt{st_{d,sc}}cosh\sqrt{st_{d,sc}/G}\right)} \tag{3}$$

where B is the relative permeability of the SC to the VE and G is the ratio of the SC to VE diffusion times (or equivalently lag times). B and G are defined in Eq. 4 and 5 respectively [28]:

$$B = \frac{k_{p,sc}}{k_{p,ve}} \tag{4}$$

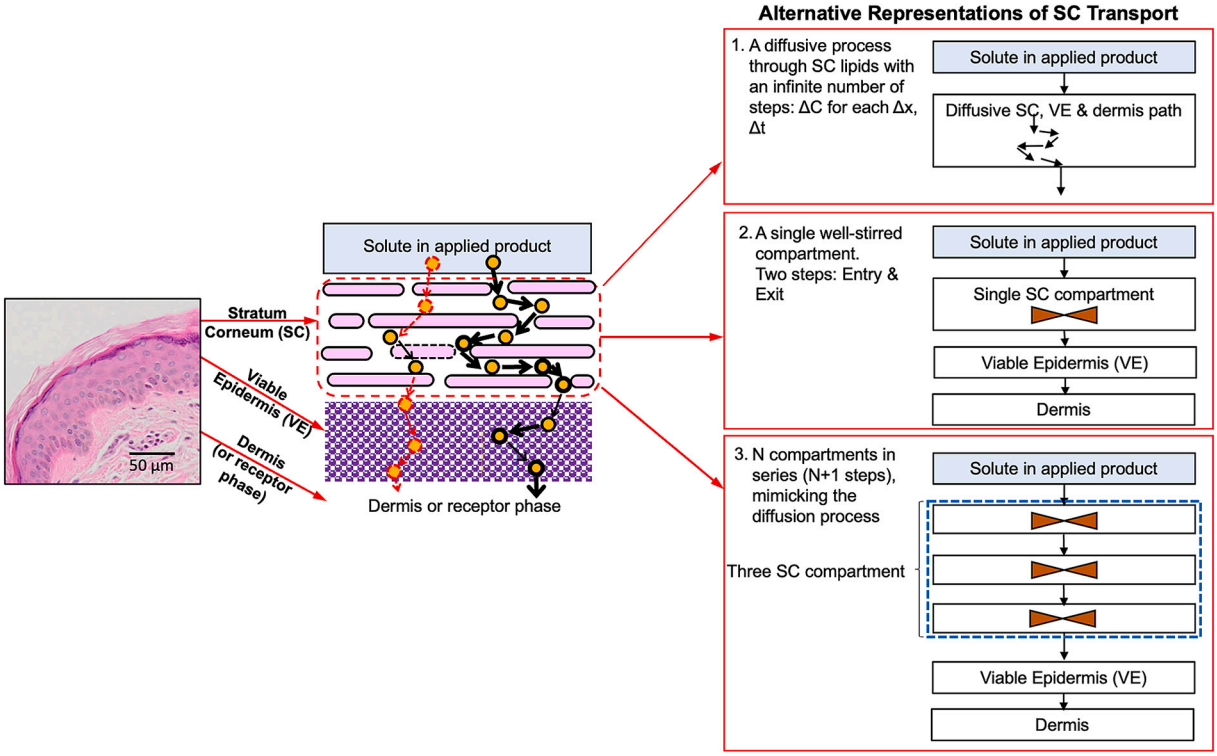

Fig. 1. Illustration of the diffusion of solute through human skin and alternative representations of solute transport through a SC barrier.

$$G = \frac{lag_{sc}}{lag_{ve}} \tag{5}$$

where $k_{p,sc}$ and $k_{p,ve}$ are permeability coefficient of SC and VE, respectively. For solutes with much greater permeability in VE compared to SC (B and $1/G$ are very small), Eq. 3 will be reduced to Eq. 1. The corresponding expression of $J_{epi}(t)$ in the Laplace domain, $\widehat{J}_{epi}(s)$, is given by:

$$\widehat{J}_{epi}(s) = \frac{J_{ss,sc}\sqrt{st_{d,sc}}}{s\left(B\frac{\sqrt{st_{d,sc}}}{\sqrt{st_{d,sc}/G}}cosh\sqrt{st_{d,sc}}\,sinh\sqrt{st_{d,sc}/G} + sinh\sqrt{st_{d,sc}}\,cosh\sqrt{st_{d,sc}/G}\right)} \tag{6}$$

Assuming a one (plasma) compartment disposition for a solute, the expression for change in its plasma concentration with time ($dC(t)/dt$) with a flux ($J(t)$) of a solute across an area into the body for both SC and epidermal limited transport is given by:

$$\frac{V_d dC(t)}{dt} = -k_{el}V_d C + J(t)A = -CLC + J(t)A \tag{7}$$

where $C(t)$ is the plasma concentration, V_d is the volume of distribution for the plasma compartment, k_{el} represents the elimination rate constant in the body and CL ($=k_{el}\,V_d$) is the plasma clearance. Eq. 7 can be solved by Laplace transforms, which yields Eq. 8 for $\widehat{C}(s)$ with the initial condition that $C(t) = 0$ at $t = 0$:

$$\widehat{C}(s) = A\widehat{J}(s)\frac{1}{(s+k_{el})}\frac{1}{V_d} \tag{8}$$

In the specific case of a one-layer SC diffusion limited flux (defined by Eq. 2, Model A(i)), the Laplace expression for plasma concentration $\widehat{C}_{sc}(s)$ is given by Eq. 9:

$$\widehat{C}_{sc}(s) = \frac{AJ_{ss,sc}}{s}\frac{\sqrt{st_{d,sc}}}{sinh\sqrt{st_{d,sc}}}\frac{1}{(s+k_{el})}\frac{1}{V_d} \tag{9}$$

For a two-layer epidermal diffusion limited flux (defined by Eq. 6, Model A(ii)), the Laplace expression for plasma concentration $\widehat{C}_{epi}(s)$ is given by Eq. 10:

$$\widehat{C}_{epi}(s) = \frac{AJ_{ss,sc}\sqrt{st_{d,sc}}}{s\left(B\frac{\sqrt{st_{d,sc}}}{\sqrt{st_{d,s}/G}}cosh\sqrt{st_{d,sc}}\,sinh\sqrt{st_{d,sc}/G} + sinh\sqrt{st_{d,sc}}\,cosh\sqrt{st_{d,sc}/G}\right)}\frac{1}{(s+k_{el})}\frac{1}{V_d} \tag{10}$$

The plasma concentration for more complex disposition models after topical and transdermal delivery can also be analysed using a similar approach. The Laplace expression for the plasma concentration with two compartment disposition models with an elimination rate constant from the plasma compartment of k_{10} and inter-compartment rate constants k_{12} and k_{21} is:

$$\widehat{C}(s) = A\widehat{J}(s)\frac{s+k_{21}}{[(s+k_{10}+k_{12})(s+k_{21}) - k_{12}k_{21}]}\frac{1}{V_d} \tag{11}$$

The corresponding expression for a three-compartment disposition model with elimination rate constant k_{10} and inter-compartment rate constants k_{12}, k_{21}, k_{13} and k_{31} is:

$$\widehat{C}(s) = A\widehat{J}(s)\frac{(s+k_{21})(s+k_{31})}{[(s+k_{10}+k_{12})(s+k_{21})(s+k_{31}) - k_{12}k_{21}(s+k_{31}) - k_{13}k_{31}(s+k_{21})]}\frac{1}{V_d} \tag{12}$$

2.1.2. Reduced steady-state skin flux diffusion models (model B)

When steady-state flux is reached, the reduced or asymptotic form of the diffusion equation for long times (defined by the singularity at $s = 0$) is described by linear relationships between $Q_{sc}(t)$ and $Q_{epi}(t)$. These reduced expressions are linear relationships described by $Q_{sc,\,linear}(t)$ and $Q_{epi,\,linear}(t)$ and as expressed in Eq. 13 and 14, respectively.

$$Q_{sc,linear}(t) = \begin{cases} 0\ (0 < t \le lag_{sc}) \\ J_{ss,sc}A(t - lag_{sc})\ (t > lag_{sc}) \end{cases} \tag{13}$$

$$Q_{epi,linear}(t) = \begin{cases} 0\ (0 < t \le lag_{epi}) \\ J_{ss,epi}A(t - lag_{epi})\ (t > lag_{epi}) \end{cases} \tag{14}$$

where the *epi*dermal steady-state flux $J_{ss,epi}$ and epidermal lag time (lag_{epi}) are defined by the relative permeability of the SC to the VE, B (Eq. 4) as:

$$J_{ss,epi} = \frac{J_{ss,sc}}{1+B} \tag{15}$$

$$lag_{epi} = \frac{lag_{sc}(1+3B)}{1+B} \tag{16}$$

Eq. 16 is only applicable when the diffusion time in VE is much shorter compared to $t_{d,sc}$ (*i.e.*, G is infinite).

Steady-state SC and epidermal flux *in vivo* diffusion models can be derived by convolution of a constant input rate of $J_{ss}A$ (Laplace solution $J_{ss}A/s$, $J_{ss,sc}$ for *IVPT* and $J_{ss,epi}$ for epidermal *in vivo* diffusion model) with the one compartment disposition function. The expression of plasma concentration in Laplace domain is shown as below:

$$\widehat{C}(s) = \frac{J_{ss}A}{s(s+k_{el})V_d} \tag{17}$$

The Laplace inversion of this expression and the inclusion of a lag time prior to steady-state diffusion yields:

$$C(t) = \begin{cases} 0\ (0 < t \le lag_{epi}) \\ \frac{J_{ss}A}{k_{el}V_d}\left(1 - e^{-k_{el}\left(t - lag_{epi}\right)}\right)\left(t > lag_{epi}\right) \end{cases} \tag{18}$$

where $lag_{epi} \sim lag_{sc}$ when SC is rate limiting. Noting $k_{el}V_d$ equals plasma clearance CL, Eq. 18 can also be expressed in the more common pharmacokinetic notation for plasma concentrations $C(t)$ for a constant input rate R_o ($=J_{ss}A$):

$$C(t) = \frac{R_o}{CL}\left(1 - e^{-k_{el}(t - lag)}\right)\ \left(t > lag_{epi}\right) \tag{19}$$

2.1.3. Full (model C) and simplified (model D) skin compartment-in-series models

We have previously developed skin compartment-in-series solutions that were in good agreement with solutions for the diffusion model of skin transport [27]. The rate constants for exchange between skin compartment-in-series were derived from physiologically relevant diffusional transport parameters. In this study, we assumed a constant solute concentration in the applied product (the donor) and used three skin compartment-in-series representing the SC (Fig. 2), as that provides an adequate approximation of the diffusion model [27]. Transport between the donor (product) and the skin can be expressed as a constant

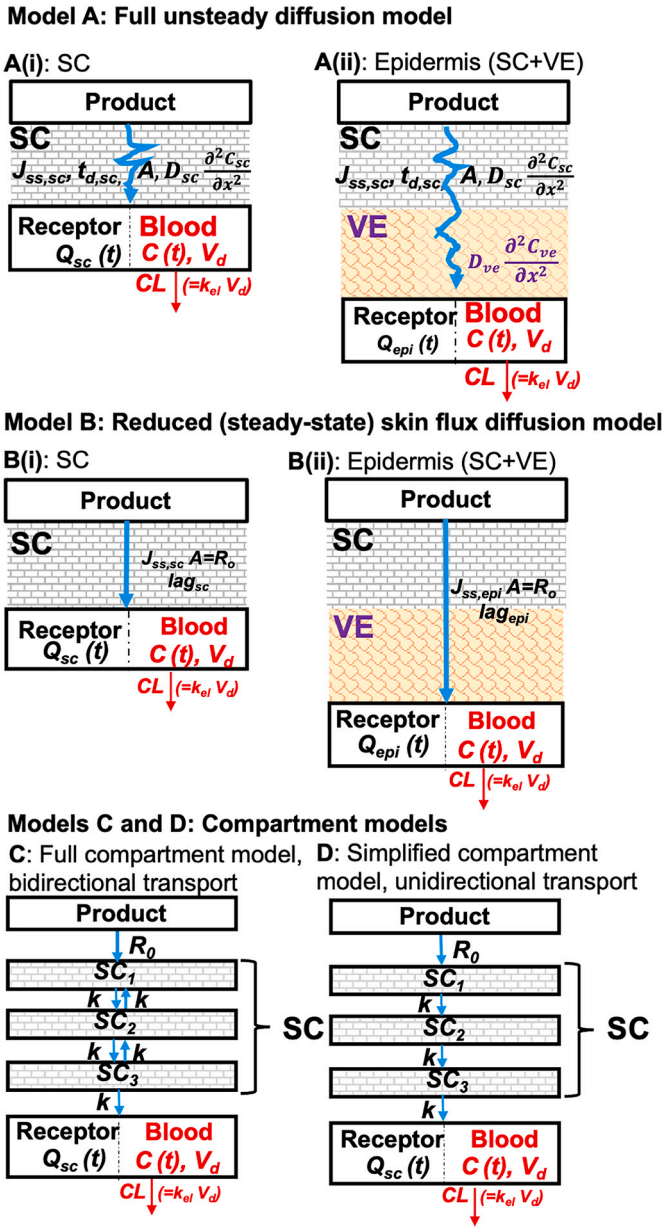

Fig. 2. Alternative models for analysing skin permeation after topical drug application. Each model can be used to predict either cumulative amount permeated into receptor ($Q(t)$, *in vitro* situation) or plasma concentration ($C(t)$, *in vivo* situation). SC- stratum corneum, VE- viable epidermis.

input rate (R_0) when there is negligible back flux from SC1. The transport between each skin compartment is defined by a rate constant k. We consider below the forward and backward bidirectional transport between skin compartments (Model C) as well as forward only unidirectional transport (Model D) (Fig. 2) mass balance equations for Model C (Fig. 2) are:

$$\frac{dSC_1}{dt} = R_0 - kSC_1 + kSC_2;$$
$$\frac{dSC_2}{dt} = kSC_1 - 2kSC_2 + kSC_3;$$

and

$$\frac{dSC_3}{dt} = kSC_2 - 2kSC_3 \tag{20}$$

where SC_1, SC_2, and SC_3 represent solute amounts in each compartment at time t. The corresponding simplified mass balance equations for forward transport only between compartments (Model D) are:

$$\frac{dSC_1}{dt} = R_0 - kSC_1;$$
$$\frac{dSC_2}{dt} = kSC_1 - kSC_2; \tag{21}$$
$$\text{and}$$
$$\frac{dSC_3}{dt} = kSC_2 - kSC_3$$

In both models, the mass balance for the receptor compartment can be expressed as:

$$\frac{dQ_{sc}(t)}{dt} = kSC_3 \tag{22}$$

where $Q_{sc}(t)$ is equal to the cumulative amount permeated through SC ($Q_{sc}(t)$) in the diffusion model. The initial conditions used here are $SC_1 = SC_2 = SC_3 = Q_{sc} = 0$. Under *in vivo* conditions, in the simplest case for a one (plasma) -compartment solute disposition, the mass balance in the plasma compartment (equal to receptor compartment in *IVPT*) can be expressed as:

$$\frac{dX_c}{dt} = kSC_3 - k_{el}X_c \tag{23}$$

where X_c is the amount of solute in the central (plasma) compartment, SC_3 is the amount of solute in third skin compartment-in-series and k_{el} is the elimination rate constant. Recognising that $X_c = C(t).V_d$, where V_d is volume of distribution of solute in the body, Eq. 23 can be re-expressed in terms of the plasma concentration of solute ($C(t)$) at any given time t:

$$V_d\frac{dC(t)}{dt} = kSC_3 - CLC(t) \tag{24}$$

The plasma concentration $C(t)$ for the reduced form of the skin compartment-in-series model can be shown to be identical to the reduced steady-state skin flux diffusion models as described by Eq. 18 and 19 when $t > lag_{sc}$, as described in B(i) and $t > lag_{epi}$, as described in B (ii). In this reduced model, there is constant rate of absorption from the third skin compartment into the plasma compartment after the lag time. This can be seen when $\frac{dSC_1}{dt} = \frac{dSC_2}{dt} = \frac{dSC_3}{dt} = 0$ so that $kSC_3 = R_o$ on substituting Eq. 19 into Eq. 18.

The corresponding mass balance equation for the amount in central (plasma) compartment X_c and in the peripheral compartment X_p for a two compartment disposition model with an elimination rate constant from the plasma compartment of k_{10}. inter-compartment rate constants k_{12} and k_{21} is:

$$\frac{dX_c}{dt} = V_d\frac{dC(t)}{dt}$$
$$= kSC_3 - (k_{10} + k_{12})V_dC(t) + k_{21}X_p \tag{25}$$

For a three-compartment disposition model with elimination rate constant k_{10} and inter-compartment rate constants k_{12}, k_{21}, k_{13} and k_{31}, with amounts of solute in the peripheral compartment 1 and 2 given by X_{p1} and X_{p2}, the mass balance equations for the central (plasma) X_c and other compartment are:

$$\frac{dX_c}{dt} = V_d\frac{dC(t)}{dt}$$
$$= kSC_3 - (k_{10}X_c + k_{12} + k_{13})V_dC(t) + k_{21}X_{p1} + k_{31}X_{p2} \tag{26}$$
$$\frac{dX_{p1}}{dt} = k_{12}V_dC(t) - k_{21}X_{p1}$$
$$\frac{dX_{p2}}{dt} = k_{13}V_dC(t) - k_{31}X_{p2}$$

In all *in vivo* cases, the initial conditions assumed here are $SC_1 = SC_2 = SC_3 = C(t) = 0$, with the amounts in the peripheral compartments (when applicable) also equal to zero. In principle, Models C and D could be easily extended to include a compartment-in-series representation of the VE and undertake a similar analysis as shown below for a combined SC-VE barrier.

2.2. Data sources

The cumulative amount permeated ($Q_{sc}(t)$) *versus* time data from *IVPT* studies performed with Nitro-Dur II® (Key Pharmaceutics) and Exelon® (Novartis) TDS were extracted from Hadgraft et al. [29] and from a publicly accessible FDA database [30], respectively using DataThief III software. For Nitro-Dur II®, dermatomed abdominal skin was used. The TDS was adhered to the SC and nitroglycerin flux through the skin were monitored over a 24 h period. For Exelon®, human skin was used and the data was extracted over a 24 h period. The corresponding plasma concentration-time profiles of nitroglycerin and rivastigmine after dermal application of these TDS were extracted from Noonan et al. [31] and FDA database [30], respectively using DataThief III. The Nitro-Dur II® TDS was applied to the upper anterior chest ($N = 24$), while the Exelon® TDS was applied to five separate sites (upper back, chest, abdomen, thigh and upper arm; $N = 35–40$).

2.3. Simulation

A series of $Q(t)$ *versus* time profiles was simulated using Model A with a range of diffusion times ($t_{d,sc}$ = 0.1, 1, 10, 30, 100, 300 and 1000 h, corresponding to lag_{sc} = 0.017, 0.17, 1.67, 5, 16.7, 50, and 167 h) and fixed steady-state flux ($J_{ss,sc}$ = 10 μg/cm^2/h), assuming a constant concentration in the donor compartment. In Model A(ii), the unsteady epidermal *IVPT* diffusion model, $t_{d,ve}$ was assumed to be 0 and the parameter *B,* describing the SC to VE permeability coefficient ratio, was varied from 0.01 to 100 with a fixed lag_{sc} of 0.17, 5 and 16.7 h. Plasma concentration ($C(t)$) *versus* time profiles were simulated for these conditions for drugs with half-lives of 1.4 h (k_{el} = 0.5 h^{-1}), 7 h (k_{el} = 0.1 h^{-1}) or 69.3 h (k_{el} = 0.01 h^{-}1) and a volume of distribution (V_d) of 10 L. Simulations were performed by Laplace inversion of Eqs. 1, 3, 9 and 10 using the program SCIENTIST® (Micro-Math Scientific Software, Missouri, US).

2.4. Data analysis

The plasma concentration-time profiles of nitroglycerin and rivastigmine after dermal application of Nitro-Dur II® (Key Pharmaceutics) and Exelon® (Novartis) TDS respectively, were analysed with Model A (i) (Laplace inversion of Eq. 9) to obtain estimated *in vivo* permeation steady-state fluxes ($J_{ss,sc}$) and lag times (lag_{sc}). The area of application A was fixed to 20 and 10 cm^2 for nitroglycerin and rivastigmine respectively, based on the properties of the TDS; k_{el} was fixed to 18.4 and 0.462 h^{-1} and V_d to 123 and 158 L, based on reported pharmacokinetic parameters after intravenous dosing of these drugs, respectively [32,33]. These datasets were also analysed by Model B, the reduced steady-state flux *in vivo* diffusion model based on Eqs. 18 and 19 and the compartment-in-series models (Model C and D). *In vitro* steady state fluxes ($J_{ss,sc}$) and lag times (lag_{sc}) were obtained by fitting *IVPT* profiles of Nitro-Dur II® and Exelon® using Model A(i) by Laplace inversion of Eq. 1.

2.5. Development of transdermal IVIVR

2.5.1. One stage convolution approach

Plasma concentration-time profiles of solutes were predicted from the convolution of *IVPT* and intravenous disposition profiles for a given solute. The *IVPT* profile was defined by fitting solute *IVPT* data with the compartment model (Model D) to yield a constant (zero-order) rate of absorption R_o (normalised by the respective delivery area) and diffusion rate constant k. A one-exponential (*i.e.* one plasma compartment) disposition model was derived from fitting of solute plasma concentration-time profiles obtained after intravenous dosing. The predicted plasma level profiles of solutes were then expressed as mean ± 90% prediction interval (upper 95% and lower 5% percentile) using the SIM function in ADAPT5 [34] and assuming each parameter had a 10% variability. These predicted profiles were then compared to the corresponding observed plasma concentration-time profiles to assess internal predictability.

2.5.2. Two stage deconvolution approach

Deconvolution of the PK data was performed using the Wagner-Nelson method [35] since the disposition of these solutes after intravenous injection followed a mono-exponential decay. The time course of the cumulative amount absorbed *in vivo* was obtained from plasma concentration data for nitroglycerin and rivastigmine after dermal application of TDS. A point-to-point *IVIVR* for each TDS was developed by linear regression of the calculated *in vivo* cumulative amount absorbed *versus* the corresponding cumulative amount permeated obtained from *IVPT* studies.

2.6. External validation

For external validation, *IVPT* data for different nitroglycerin TDS, Deponit® (Schwarz Pharma), Transderm-Nitro® (Ciba Geigy) and Minitran®(3 M Riker) were obtained from Hadgraft [29]. The characteristics of these TDS are summarized in Table 1 [29]. Dermatomed abdominal skin was used and nitroglycerin flux through the skin were monitored over a 24 h period.

IVPT data were then converted to *in vivo* cumulative amount absorbed by multiplying the set of regression parameters corresponding to *IVIVR* developed previously. The prediction of *in vivo* nitroglycerin plasma concentrations from corresponding *in vivo* absorption profiles was accomplished by convolution of the *in vivo* flux and disposition profiles using Model D. The predicted parameters C_{ss} and $AUC_{0\text{-}last}$ were compared to those reported in the literature for *in vivo* studies performed with the same TDS [36] to determine prediction errors (*%PE*). The percentage prediction error (*%PE*) was calculated as follows:

$$\%PE = \frac{Observed - Predicted}{Predicted} \times 100\% \quad (27)$$

3. Results

3.1. Impact of model parameter variation on skin permeation and in vivo plasma concentration - time profiles

Fig. 3 shows simulated time profiles of *in vitro* SC permeation ($Q_{sc}(t)$) (Fig. 3I) and the corresponding *in vivo* plasma concentration (Fig 3II-IV) using the full unsteady diffusion model (Model A(i)) under *in vitro* and *in vivo* situations, respectively. Solutes were assumed to have steady-state SC permeation fluxes ($J_{ss,sc}$) of 10 μg/cm^2/h and a range of SC lag times. Each of the $Q_{sc}(t)$ *versus* time plots shows an initial curvature followed by a linear phase. The most important impact of increasing lag_{sc} in the *in vitro* studies was a correspondingly longer delay in the time taken for solute to appear in the receptor phase and for the attainment of steady-state permeation (the linear phase of the plot). In the *in vivo* situation, increasing lag_{sc} results in an increased time to reach maximum plasma concentrations, whereas the magnitude of this maximum concentration is independent of lag_{sc} (Fig. 3II-IV). Regardless of the lag time, when the elimination rate constant (k_{el}) is increased, the maximum plasma concentrations are proportionally lower, but this maximum concentration is achieved more rapidly (Fig. 3, II *vs* III and IV).

Table 1
Characteristics of the investigated nitroglycerin TDS.

Nitroglycerin Patch	Area (cm^2)	Total Drug (mg)	Claimed *in vivo* delivery rate (mg/24 h)
Nitrodur	20	80	10
Deponit	32	32	10
Transderm Nitro	20	50	10
Minitran	13.3	36	10

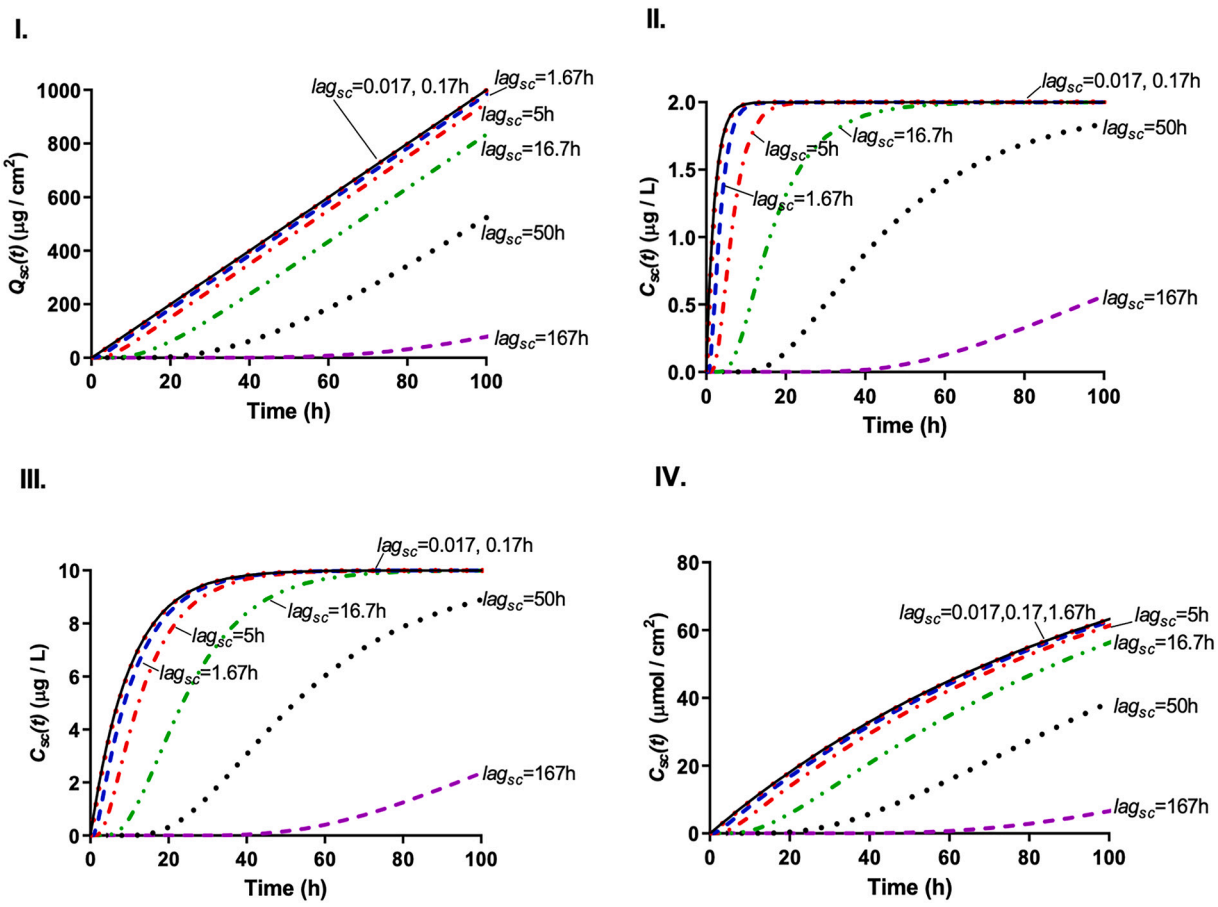

Fig. 3. Simulated cumulative amounts of solute permeated through stratum corneum ($Q_{sc}(t)$) *versus* time profiles (**I**) and corresponding plasma concentration ($C_{sc}(t)$) *versus* time profiles (**II-IV**) for continuously applied solutes using the full diffusion Model A(i). A steady-state SC permeation flux ($J_{ss,sc}$) of 10 µg/cm^2/h and SC diffusion lag times (lag_{sc}) of 0.017, 0.17, 1.67, 5, 16.7, 50 and 167 h were used in all simulations. Elimination rate constants (k_{el}) of 0.5 h^{-1}, 0.1 h^{-1} and 0.01 h^{-1} were applied in simulations shown in **II**, **III** and **IV** respectively, to represent fast ($t_{1/2}$ = 1.4 h), moderate ($t_{1/2}$ = 6.9 h) and slow ($t_{1/2}$ = 69 h) elimination, with a volume of distribution (V_d) of 10 L.

Fig. 4 shows simulations of $Q_{epi}(t)$ and $C_{epi}(t)$ *versus* t profiles using the full unsteady diffusion model (Model A(ii)) for a range of SC to VE permeability coefficient ratios, B (Eq. 4). Here, it is noted that when the VE is infinitely permeable, the parameter $B = 0$ and the $Q_{epi}(t)$ and $C_{epi}(t)$ profiles are identical to the $Q_{sc}(t)$ and $C_{sc}(t)$) profiles shown for a one phase SC barrier in Fig. 2. When the VE is much more permeable than SC, as reflected by a small B ($B = 0.01$), the simulated $Q_{epi}(t)$ and $C_{epi}(t)$ profiles are almost identical to those for $B = 0$. With the increase of B, the $Q_{epi}(t)$ were dramatically decreased, indicating greater hindrance to solute from the SC flux entering and passing through the VE. Fig. 4II and III show the corresponding *in vivo* $C_{,epi}(t)$ profiles for $k_{el} = 0.5$ (Fig. 4II) and 0.1 h^{-1} (Fig. 4III). Here, the effect of B on $C_{epi}(t)$ is, in relative terms, similar for the different lag times and for the two k_{el} values. The overall effect is a decrease in $C_{epi}(t)$ with an increase in B and these changes are further enhanced by an increase in SC lag and/or an increase in k_{el}. In the extreme case for very lipophilic solutes with $B \geq 100$, the VE barrier may be so effective that almost no solute can permeate the epidermal membrane under *in vitro* conditions or appear in the plasma after *in vivo* topical application.

3.2. Diffusion modelling of in vivo plasma concentrations after TDS application

Fig. 5 shows a comparison of the non-linear regression of experimental nitroglycerin and rivastigmine plasma levels *versus* time following TDS application at various body sites, using the full diffusion Model A(i), reduced diffusion model B(i), the full skin compartment-in-series model C and a simplified skin compartment-in-series model D. It is apparent that the full diffusion Model A(i) and the two skin compartment-in-series models adequately describe the data, but the approximate diffusion model, Model B(i) (and, not shown as it is identical to B(i), reduced compartment-in-series models), poorly describe the data at early times, up to 5 h. Data presented in Fig. 5 suggest that the simplest model that adequately describes the experimental data is the approximate and simplified compartment-in-series model, Model D, in which transport is assumed to be unidirectional.

Table 2 presents a comparison of the *in vitro* and *in vivo* skin steady-state permeation fluxes ($J_{ss,sc}$) and lag times (lag_{sc}) for both drugs. Here it can be seen that for both nitroglycerin and rivastigmine, the derived *in vitro* and *in vivo* values of $J_{ss,sc}$ are comparable, while a difference in lag_{sc} is seen for nitroglycerin. The derived values of $J_{ss,sc}$ for rivastigmine are comparable at different body sites, whereas the diffusional lag time obtained for the thigh is greater than for the other body sites (7.47 h, compared to 3.87–5.00 h at other sites). This observation is supported by the different plasma concentration-time profile obtained for the thigh, which appears to reach steady state later than the profiles obtained after application to other body sites (Fig. 5).

3.3. Transdermal IVIVR

The convolution of the *IVPT* data (Fig. 6A, k = 10.1 h^{-1} and R_0 = 446.9 µg/h for nitroglycerin, k = 0.677 h^{-1} and R_0 = 379.8 µg/h for rivastigmine) and the intravenous plasma disposition profiles of each drug using the compartment-in-series *in vivo* solution yields the

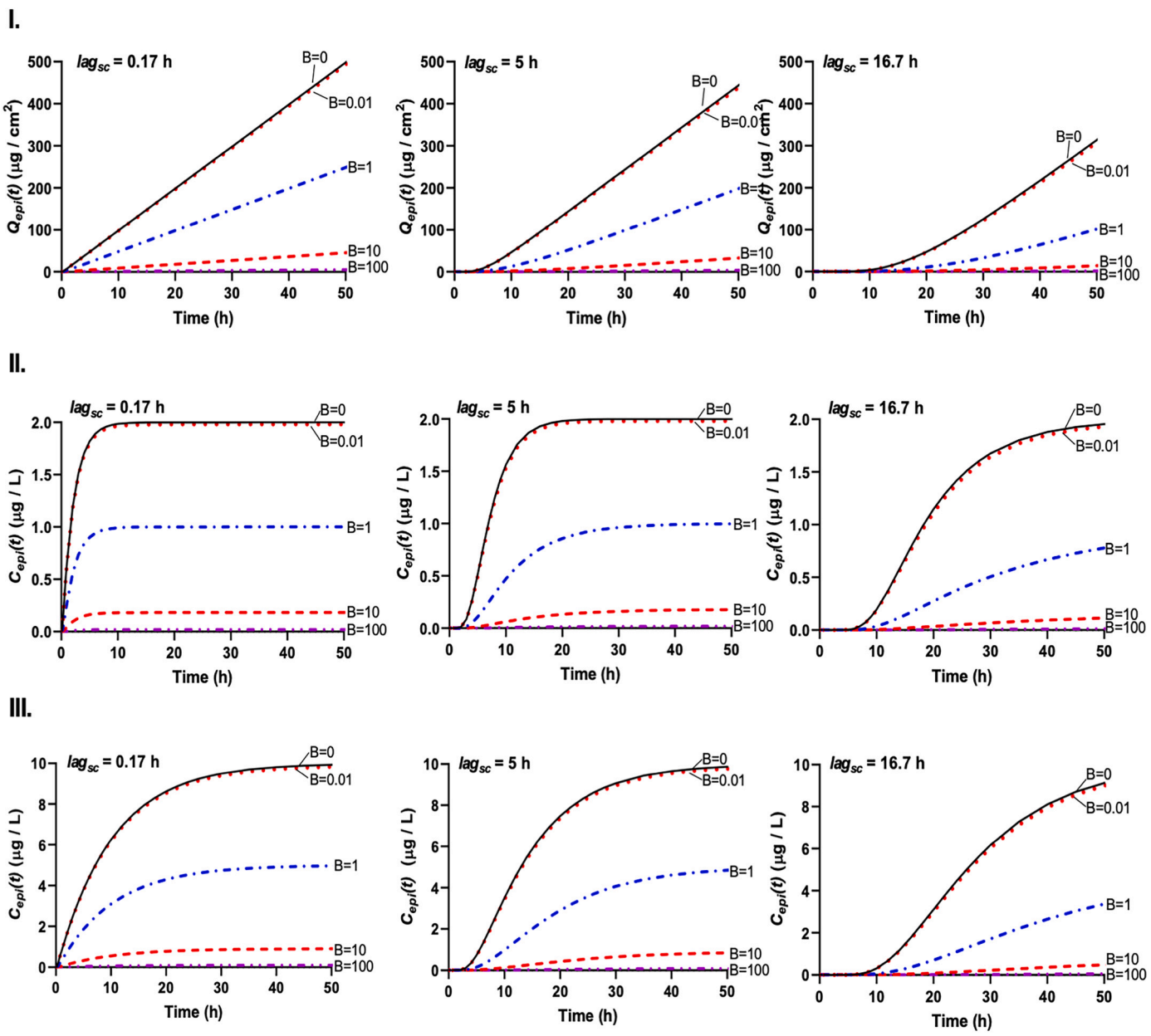

Fig. 4. Simulated cumulative amounts permeated through epidermis ($Q_{epi}(t)$) *versus* time profiles for continuously applied solutes **(I)** and corresponding plasma concentration ($C_{epi}(t)$) *versus* time profiles for continuously applied solutes using the unsteady epidermal *in vivo* diffusion model **(II** and **III))** using Model A(ii). The simulations were based on a steady-state SC permeation flux ($J_{ss,sc}$) of 10 µg/cm^2/h and SC diffusion lag times (lag_{sc}) of 0.17, 5 and 16.7 h, assuming a value of 0 for $t_{d,ve}$. The *in vivo* simulations were performed with elimination rate constants (k_{el}) of 0.5 h^{-1} **(II)** and 0.1 h^{-1} **(III)** and a volume of distribution (V_d) of 10 L. Each panel shows the effect of the parameter *B,* the ratio of the SC to VE permeability coefficients, on $Q_{epi}(t)$ and $C_{epi}(t)$.

predicted plasma concentration-time profiles with 90% prediction intervals shown in Fig. 6B. It is evident that the experimental plasma concentration-time profiles after dermal application of nitroglycerin and rivastigmine TDS fall within the 90% prediction intervals obtained from convolution. Fig. 6C shows results of linear regression performed for the estimated *in vivo* absorption (obtained by deconvolution of experimental plasma concentration-time profiles using the Wagner-Nelson method) *versus* the *in vitro* cumulative amount permeated (obtained from the *IVPT* data shown in Fig. 6A. A linear relationship was found, with $r^2 >$ 0.99 and a slope close to unity for both solutes.

The prediction errors (*%PE*) for the global parameters of steady state plasma concentration C_{ss} and area under the curve for the sampling period ($AUC_{0\text{-}last}$) are summarized in Table 3. The absolute *%PE* was less than 15% for all the parameters of dermal nitroglycerin and rivastigmine delivery except for the case where rivastigmine was applied to the thigh.

3.4. External validation

As external validation data sets, we chose *IVPT* study profiles reported in the literature for three different nitroglycerin TDS tested in the same laboratory, using dermatomed abdominal skin [29]. The *in vivo* plasma concentration-time profiles for the same product were extracted from literature as well [36]. The external validation results are presented in Fig. 7 and summarized in Table 4. The PE% of Minitran® was −58.3% for C_{ss} and − 54.9% for $AUC_{0\text{-}last}$, well outside the acceptable range of 20% according to FDA guidance [37], and thus failing to pass external validation. Deponit® and Transderm-Nitro® were close to passing external validation, as their %PE values for both C_{ss} and $AUC_{0\text{-}last}$, were just outside the acceptable 20% range (−22.1%, −26.7% and

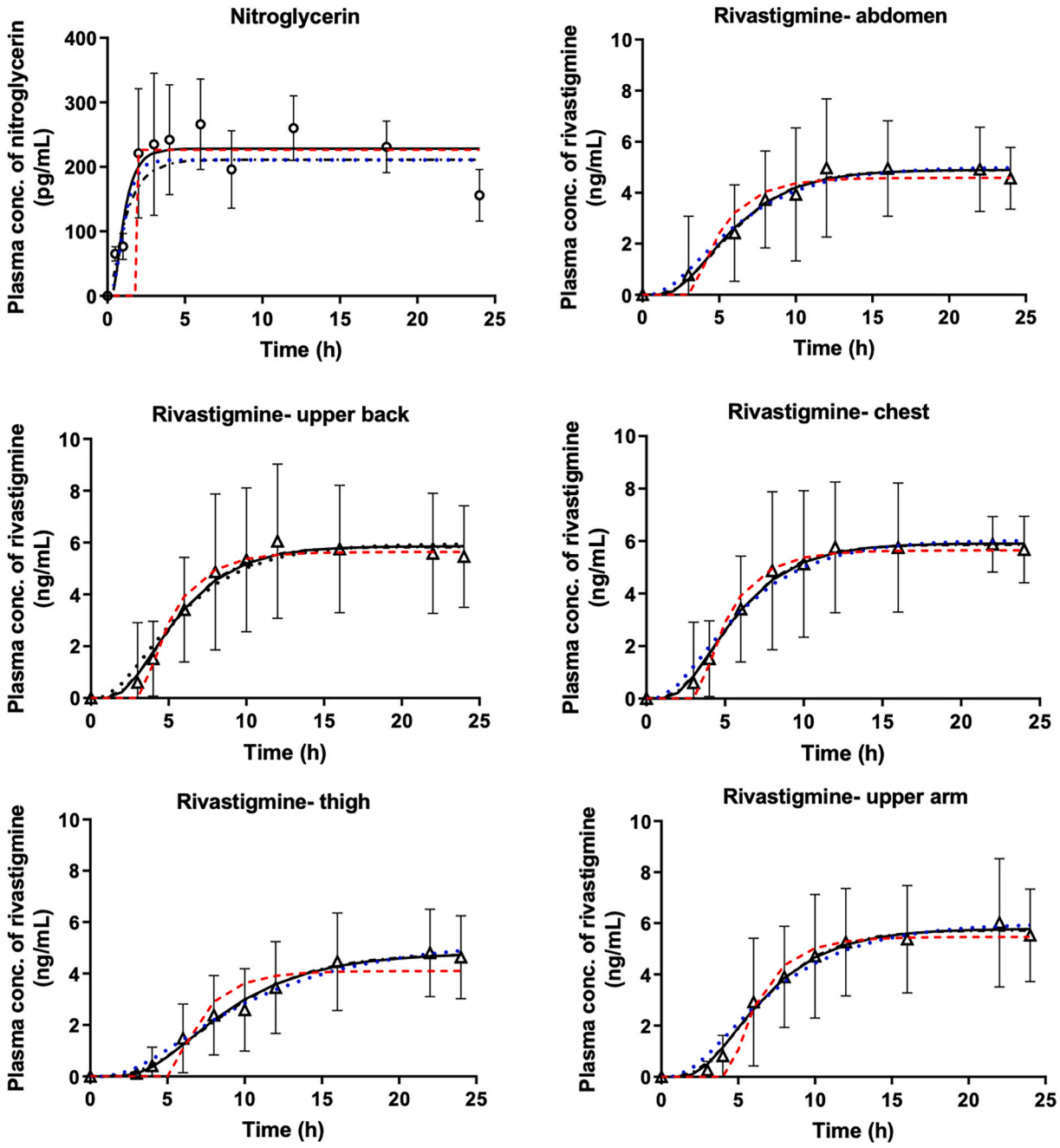

Fig. 5. Non-linear regression fitting of plasma concentration *vs* time profiles after topical application of nitroglycerin and rivastigmine from transdermal patches. Rivastigmine was applied at the five body sites indicated. Open symbols represent experimental data obtained from literature [31] and a publicly accessible FDA database [30]. Fittings obtained from pharmacokinetic models described in Fig. 2 are shown as black solid lines (Model A(i), using Laplace inversion of Eq. 10); red dashed lines (Model B(i), Eq. 19); blue dotted lines (Model C); black dash-dotted lines (Model D). (For interpretation of the references to colour in this figure legend, the reader is referred to the web version of this article.)

− 21.5%, −23.2% for Deponit® and Transderm-Nitro® respectively).

4. Discussion

A key goal underpinning the present work was to develop pharmacokinetic models and related methodology for precise and accurate prediction of *in vivo* plasma concentration – time profiles from *IVPT* studies, in order to evaluate the pharmacokinetics of products applied to the skin. Currently, the *in vivo* absorption of most dermally applied products and solutions is simply reported as the percentage of the dermally applied dose excreted into the urine, or a first or zero order absorption process is often assumed [38–40]. While there are a number of pharmacokinetic models that have been used to describe percutaneous permeation, these have generally been limited to the analysis of *IVPT* data and most are based on a diffusion limited process in the SC, and to a lesser extent, the epidermis, dermis and deeper tissues. As the resulting equations describing the percutaneous absorption process are generally complex, studies have been undertaken using a large ("infinite") dose, in which there is a minimal change in the thermodynamic activity of the solute in the applied vehicle, and analysed in terms of the cumulative amount permeated during the steady state phase. The choice of these conditions allows the experimental data to be analysed using the steady-state flux diffusion model (Model B(i) described by Eq. 13). In this work, we developed pharmacokinetic models to describe *in vivo* plasma

Table 2
Summary of skin steady-state permeation flux ($J_{ss,sc}$) and diffusion lag time (lag_{sc}) (mean (SD)) of nitroglycerin and rivastigmine TDS obtained by fitting *IVPT* data and plasma concentration time profiles using the full unsteady diffusion model (Model A(i)).

Drug	$J_{ss,sc}$ (μg/cm²/h)		lag_{sc} (h)	
	In vitro	*In vivo*	*In vitro*	*In vivo*
Nitroglycerin	22.3 (1.1)	25.8 (1.6)	0.30 (0.07)	1.15 (0.25)
Rivastigmine				
Upper back	38.3 (1.2)	42.8 (1.2)	4.56 (0.43)	3.87 (0.30)
Chest		43.2 (0.8)		3.98 (0.20)
Abdomen		35.8 (1.0)		4.27 (0.37)
Thigh		35.1 (1.1)		7.47 (0.40)
Upper arm		42.2 (1.0)		5.00 (0.27)

concentration – time profiles after application of TDS products to *in vivo* human skin. The models were derived in the Laplace domain as a convolution of an *in vitro* diffusion function based on *IVPT* results (and steady-state flux diffusion model and compartment-in-series model) with various disposition functions. We then examined the sensitivity of the predictions to changes in the percutaneous absorption and disposition parameters. Our analysis showed that the profiles of plasma concentration at the early times (Fig. 2B) were highly dependent on the diffusion time, with the most pronounced differences arising for the longer diffusion times. We considered a wide range of diffusion times, from 0.1 to 1000 h, to cover the short lag times reported for phenolic compounds and the long lag times seen with steroids, typified by hydrocortisone with a diffusion time of about 1000 h [41]. A key advantage of our model is its explicit representation of plasma concentrations in terms of steady state skin absorption fluxes, lag times and plasma clearance. This allows our model to be extended to predict solute

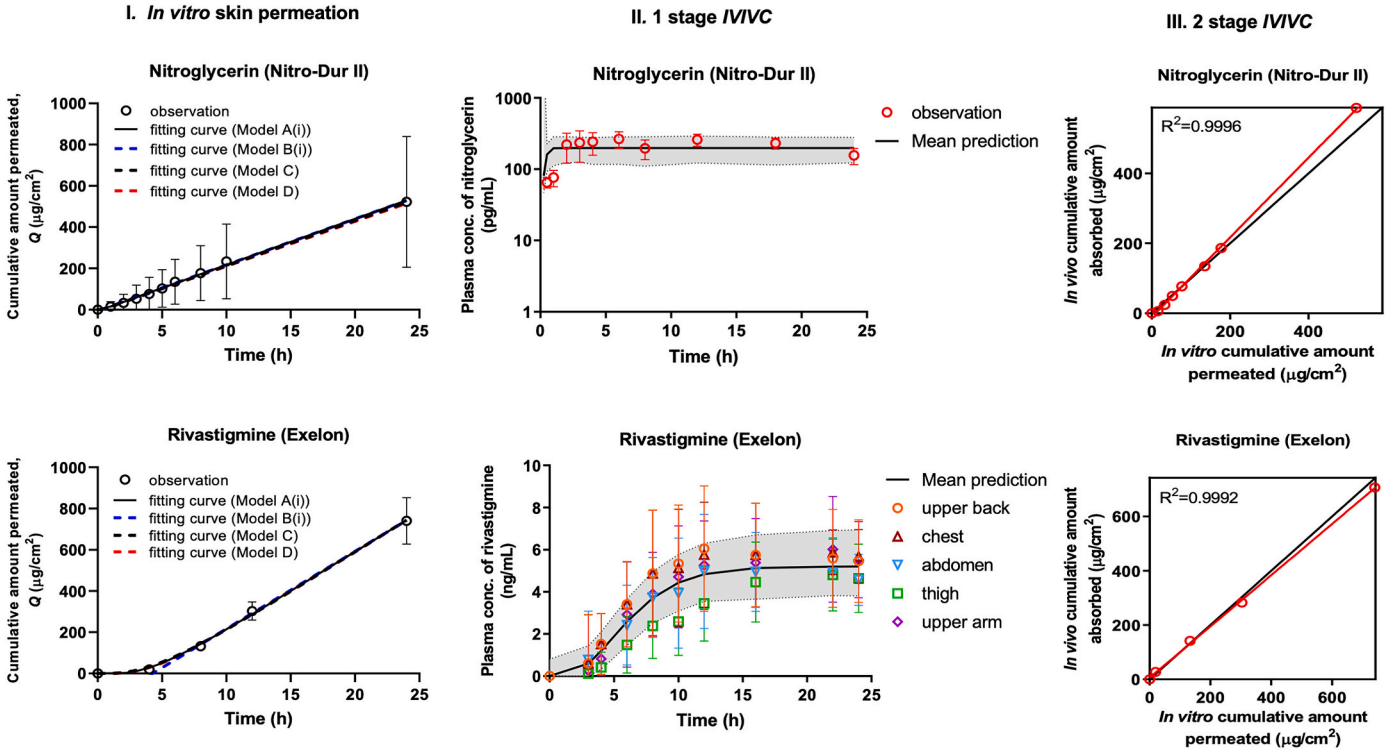

Fig. 6. *In vitro - in vivo* relationships (*IVIVRs*) of nitroglycerin and rivastigmine permeation through human skin after application of transdermal patches. **(I)** *IVPT* results, showing cumulative amounts permeated ($Q(t)$) *versus* time profiles. Symbols and error bars represent experimental data (mean ± SD) and the various lines represent fitting curves using Model A(i) (Laplace inversion of Eq. 1), Model B(i) (Eq. 13) and the two compartment-in-series models (Model C and D); **(II)** Convolution of the *IVPT* profiles with the intravenous disposition profiles using Model D to yield 90% predicted plasma concentration intervals. Observed values are shown by symbols and error bars (mean ± SD) for nitroglycerin and rivastigmine. The predicted plasma concentration-time profiles are shown as solid lines and the shaded areas represent 90% prediction intervals; **(III)** Comparison of the cumulative amounts permeated in *IVPT* studies with the estimated amounts absorbed *in vivo* using a Wagner-Nelson deconvolution of the plasma concentration – time profile for the two solutes.

Table 3
Summary of observed and predicted pharmacokinetic parameters of nitroglycerin and rivastigmine after TDS application.

Drug	C_{ss} *			$AUC_{0\text{-}last}$ **		
	Observed	Predicted	*%PE*	Observed	Predicted	*%PE*
Nitroglycerin	228	198	13.2	5183	4672	9.9
Rivastigmine						
Upper back	5.86	5.2	11.3	105.0	90.6	13.7
Chest	5.91		12.0	105.0		13.7
Abdomen	4.89		−6.34	86.5		−4.7
Thigh	4.72		−10.2	70.1		−29.2
Upper arm	5.77		9.88	96.7		6.3

* pg/mL for nitroglycerin and ng/mL for rivastigmine.
** pg/mL.h for nitroglycerin and ng/mL.h for rivastigmine.

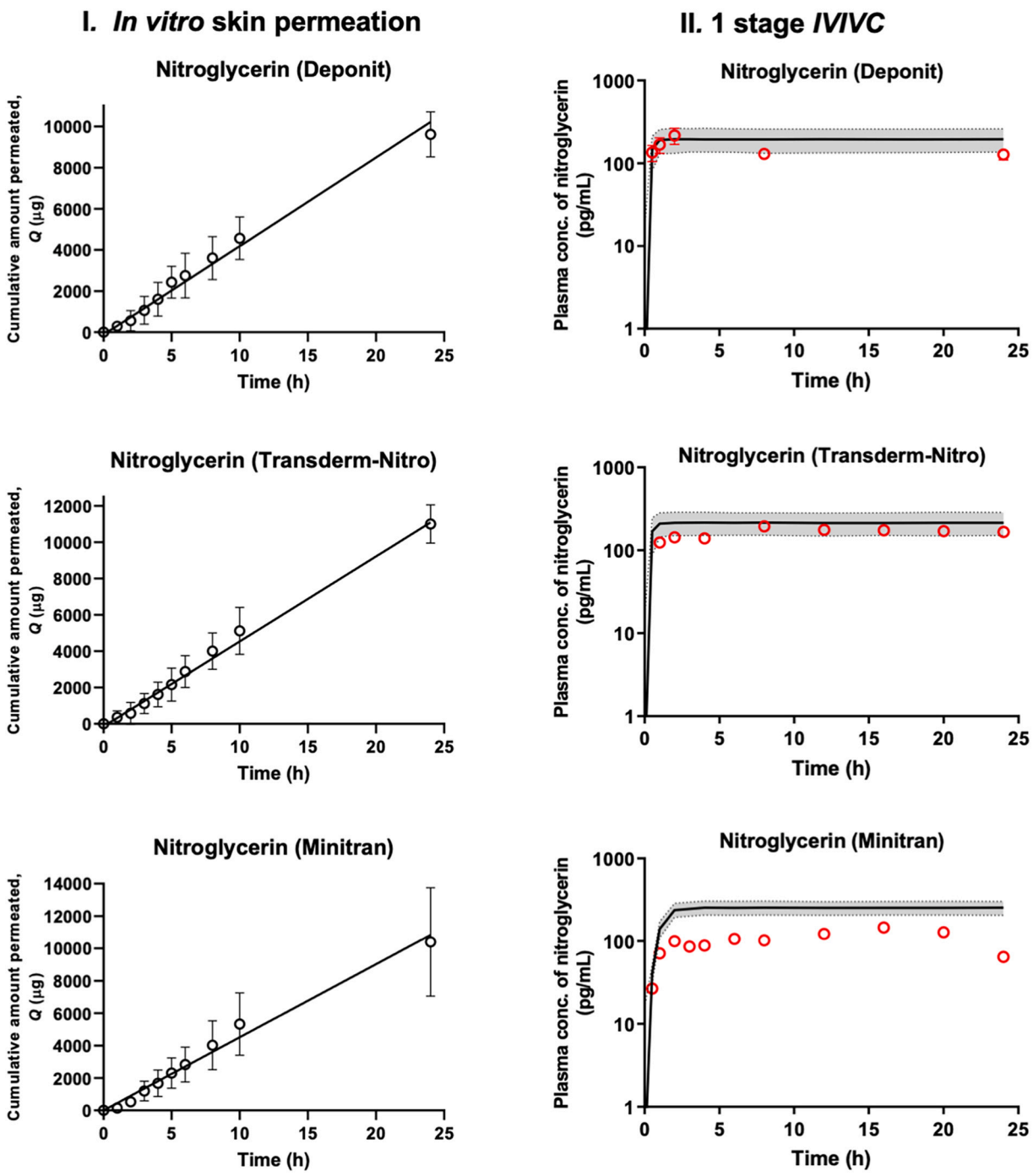

Fig. 7. External validation of *IVIVR* for nitroglycerin. (**I**) reported *in vitro* permeation test (*IVPT*) results for cumulative amount permeated (*Q(t)*) *versus* time profiles. Symbols and error bars represent experimental data (mean ± SD); lines represent fitting curves using Model D; (**II**) Convolution of the *in vivo* absorption profile (obtained from *IVPT* data prediction based on *IVIVR*) with the intravenous disposition profiles using Model D to yield 90% predicted plasma concentration intervals for nitroglycerin. Observed values are shown by symbols and error bars (mean ± SD). The predicted plasma concentration-time profile is shown as a solid line and the shaded areas represent 90% prediction intervals.

Table 4
External validation results: observed and predicted pharmacokinetic paramters for Deponit®, Transderm-Nitro® and Minitran® TDS.

TDS	C_{ss} (pg/mL)			$AUC_{0\text{-}last}$ (pg/mL.h)		
	observed	predicted	*%PE*	observed	predicted	*%PE*
Deponit®	152	195	−22.1	3373	4602	−26.7
Transderm-Nitro®	168	214	−21.5	3882	5058	−23.2
Minitran®	105	252	−58.3	2608	5782	−54.9

permeation through impaired skin if we can estimate the most likely steady flux and lag time for a TDS or topical product applied to this skin, as well as to populations in which there is a change in clearance and this is known.

We recognised that our approach of using numerical integration and Laplace transform solutions to describe the *in vivo* plasma concentration profiles and a SC diffusion models required special software (*e.g.* Scientist®) to do the model fitting of data. The numerical integration of Laplace solutions is not easily implemented on population pharmacokinetic software such as NONMEM and ADAPT5. We therefore deduced the reduced steady-state flux diffusion model and approximate compartment-in-series skin models that are either in the form of an analytical expression or a series of ordinary differential equations, which can be easily used with NONMEM or ADAPT5 (using the maximum likelihood expectation maximization, MLEM, program). The reduced steady-state flux diffusion solution (Model B) is based on the limits of the Laplace equations at long times (*i.e.*, as $t \rightarrow \infty$), whereas the skin compartment-in-series skin model (Model C and D) approximates the infinite number of forward and backward transport steps that occur in a diffusion process by a finite number of compartments, following the process we have described previously [27,42]. In this study, we tested 1–5 compartment-in-series skin models to represent SC, considering forward and backward transport or forward transport only. The goodness of fit was evaluated by visual examination of the predicted curves and comparison of AIC value. The approximate three-compartment-in-series skin model was selected on the basis of the lowest AIC and was used in the later analyses. In general, the reduced steady-state flux diffusion model poorly described plasma concentrations at early times (Fig. 5). One and two compartment-in-series skin models (to represent SC) could not adequately describe the plasma concentration profiles of solutes with long diffusion times, while the four compartment-in-series skin model was not superior to the three-compartment-in-series skin model.

We applied all derived models to predict *in vivo* plasma concentration – time profiles of two solutes, nitroglycerin and rivastigmine, that were reported previously [30,31]. We found that all models, other than the reduced steady-state flux diffusion model, gave similar predicted curves and AIC values. To develop *IVIVR*, we extracted *IVPT* data that corresponded to the *in vivo* studies from literature [29,30]. These *IVPT* data were also well described by the unsteady diffusion model and compartment-in-series skin models, but not the reduced steady-state flux model, which poorly described data at early times (Fig. 6I). The *in vitro* and *in vivo* steady state permeation parameters derived for nitroglycerin and rivastigmine appeared to be comparable (Table 2). The suitability of the uni-directional compartment-in-series skin model is consistent with a constant thermodynamic activity in the dermally applied product in the particular dosage conditions considered here - leading to subsequent concentrations in the various layers of the SC and deeper tissues decreasing with depth, and to a relatively much lower back flux.

The modelling of plasma concentration-time profiles in this work suggested that similar $J_{ss,sc}$ and lag_{sc} values were obtained after rivastigmine TDS were applied on the skin at different anatomical sites (Table 2). In contrast, anatomical site differences in skin permeation have previously been reported for salicylic acid [43], hydrophilic compounds [44], methyl salicylate [45], organic compounds [46], scopolamine [47] and contraceptive TDS [48,49], both *in vitro* [43,44] and *in vivo* [45–49]. Fig. 8 shows a comparison of the body site variations in skin absorption for a wide range of drugs [50] with SC morphology (expressed as the reciprocals of SC thickness and number of SC strata,) and SC function (TEWL, SC hydration).

It is evident that for the transdermal sites shown in Fig. 8I, there is only a small variation in SC morphology, and this is paralleled by the skin absorption of the transdermal drugs listed, with the thigh tending to be lower than the other sites. Moreover, rivastigmine $J_{ss,sc}$ parallels the plasma area under the curve *AUC* for the transdermal products shown in Fig. 8I. Of note, for this data set, the number of SC strata appears to be a better predictor for skin absorption *via* the thigh than the SC thickness, TEWL or SC hydration (conductance) (Fig. 8I). In contrast, as shown in

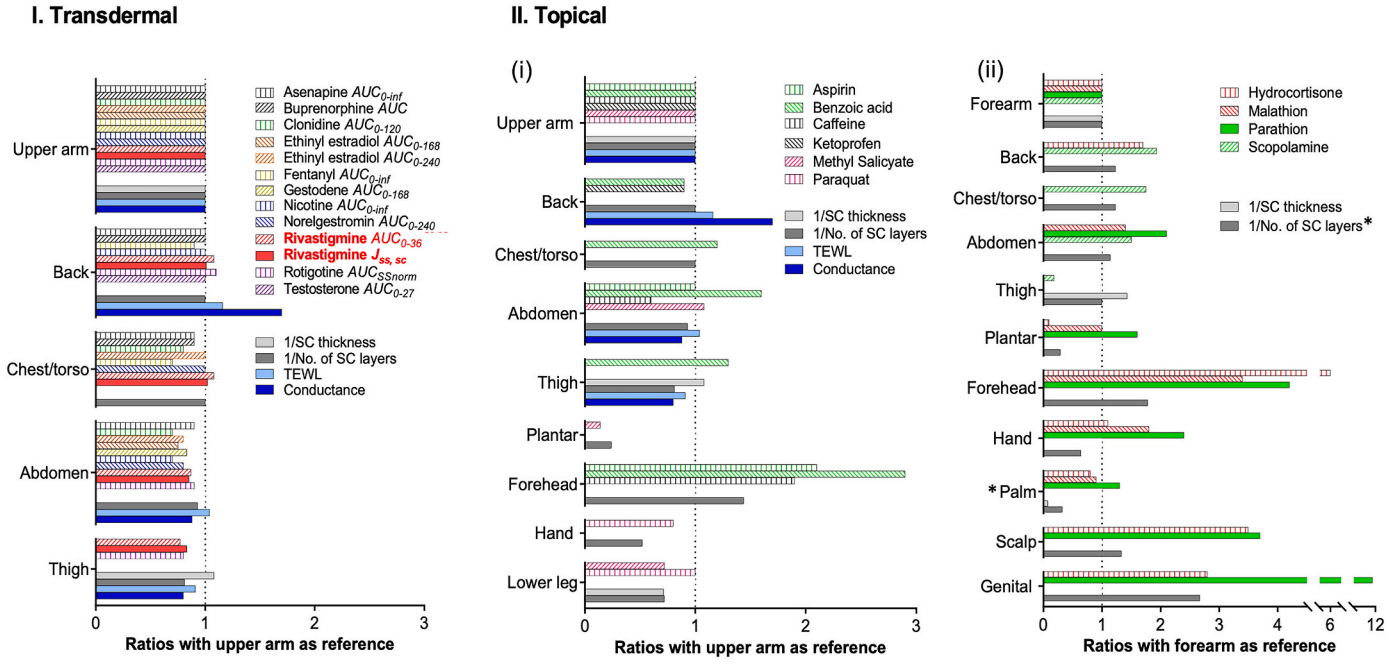

Fig. 8. Body site dependence of drug percutaneous absorption and skin physiological parameters for I. transdermal products plasma $AUC_{0-\infty}$ (and *Jss* for rivastigmine), normalised to values for the upper arm, II(i) estimated absorption of topical products, normalised to values for the upper arm and II(ii) estimated absorption of topical products, normalised to values for the forearm. Data used in Fig. 8 were obtained from the literature: Fig. 8I – Asenapine [51], Buprenorphine [52], Clonidine [53], Ethinyl estradiol [48,49], Fentanyl [54], Gestodene [49], Nicotine [55], Norelgestromin [48], Rivastigmine [30], Rotigotine [56], Testosterone [57]; Fig. 8II(i) – Aspirin [43], Benzoic acid [58], Caffeine [59], Ketoprofen [60], Methyl salicylate [45], Paraquat [44]; Fig. 8II(ii) – Hydrocortisone [61], Malathion [62], Parathion [62], Scopolamine [47]. The SC thickness values were derived from the work of Polak et al. [63], except for the palm*, which was reported by Bohling et al. [64]. Values for the number of SC layers, TEWL and conductance (SC hydration) came for a study by Ya-Xian et al. [65].

Fig. 8II (i), topically applied benzoic acid has a higher absorption for the chest, abdomen and thigh than would be predicted from the data in Fig. 8I. Further, topical absorption data for benzoic acid and other drugs show considerable variability in absorption across other body sites (noting these are not usually used for transdermal delivery) as shown in Fig. 8 II(i) and (ii) and appear to be better correlated with 1/no of SC layers than any other physiological parameter. A complicating factor in this analysis is the different distributions in age, sex and racial phenotype between the various populations and their impact on percutaneous absorption. For instance, in the studies included in this analysis, the rivastigmine population included 19 Caucasian and 20 Japanese subjects (57% female) with an age range of 51–80 yr (mean 52) [30] whereas the benzoic acid, aspirin and caffeine volunteers were all male Caucasians with a mean age of 28 ± 2 yr [43,58,59]. The measurement of SC layer numbers, TEWL and skin conductance was performed in a Japanese study where the population was 48% female, with an average age of 42 ± 26 yr [65] whereas the demographics for the SC thickness study was not disclosed [63]. The largest confounder in such comparisons as these is likely to be age, as it is well known that the SC undergoes considerable alterations with age, in which it becomes flatter and stiffer, and shows greater cellular strata cohesion and increased strata numbers. Individual corneocytes have a greater surface area, but are reduced in thickness. Other changes with ageing include a greater surface pH, increased intercellular lipid cohesion and reduced TEWL [66]. This data suggests that extrapolating the present skin absorption data beyond specific body sites commonly used in transdermal delivery based on other drug absorption data and SC physiology for a general population will have considerable uncertainty. However, as shown in Fig. 8I, the number of SC cell layers for a similar subject population may be an indicative predictor for absorption at other body sites. Fig. 8I also suggests that the bioavailability of transdermal products seen across anatomical sites generally used for these products may not be sufficiently variable to lead to detectable changes in therapeutic effects or to raise safety concerns, as seen, for example, in the systemic exposure of ethinyl estradiol and gestodene after TDS application [49]. Here, the bioavailabilities of ethinyl estradiol and gestodene were greater after TDS application to the outer, upper arm compared to the lower abdomen (Fig. 8I) and buttocks, but the differences were not regarded as clinically significant [49].

Transdermal rivastigmine and its metabolite NAP226–90 pharmacokinetics appeared to show no differences for variations in gender, race, age, multiple dosing and atopic dermatitis compared with healthy volunteers for the same patch size applied to the same site (30). However, various skin diseases have been shown to modulate skin permeation, as reviewed by Bucks [67], who pointed out that most diseases, including atopic dermatitis, sodium lauryl sulfate-induced contact dermatitis, psoriasis and physically compromised skin lead to an increased skin penetration compared to normal skin. For instance, in contrast to the rivastigmine data (30), crisaborole has recently been shown to have ~2.5-fold higher AUC_{ss} and $C_{max,ss}$ values in atopic dermatitis or psoriasis patients at a given crisaborole ointment dose relative to healthy participants [68]. TEWL values for psoriatic and atopic dermatitis lesions of ~1.5 times and ~ 2.4 times relative to non-lesional skin, respectively, have recently been reported [69]. Zainal et al. [70] noted that TEWL for atopic dermatitis lesions on the chest were ~ 3 times non-lesional areas and ~ 1.4 times higher (on average) across all body sites studied. In summary, whilst an *IVPT* study may be predictive of *in vivo* performance, it is limited by the properties of the skin used in the *IVPT* study. However, for the most commonly used transdermal application body sites, there appears to be similar absorption (Fig. 8I) with the number of SC layers and TEWL providing an indicative measure of the likely absorption at other sites (Fig. 8II) and in diseased skin, respectively. An important consideration in this extension is the relative contributions of formulation release and skin permeability in defining the skin input function.

There has been great interest in the development of *in vitro - in vivo* correlations (*IVIVC*) for extended release (*ER*) oral dosage forms [37], because dissolution data for such products might thereby be useful to evaluate the impact of various formulation and manufacturing changes, as a potential alternative to performing *in vivo* BE studies. We considered whether a similar approach might also be useful for products applied to the skin, allowing *IVPT* results to be utilized with a pharmacokinetic diffusion model to predict *in vivo* plasma concentration-time profiles. We therefore used a method that was analogous to that recommended by the FDA for extended release (ER) product *IVIVC* [37] and generated a point-to-point *IVIVR* using a one-stage convolution to predict plasma data from the skin *IVPT* profile in a single step. Linear relationships were found between the predicted and experimental skin permeation for both nitroglycerin and rivastigmine, with slopes of approximately 1 (Fig. 6), indicating that an acceptable *IVIVR* had been established for these drugs. This is consistent with the high correlation of *in vivo* and *in vitro* transdermal drug absorption that has previously been demonstrated [47,71]. However, the external validation results using other brands of nitroglycerin TDS failed to meet FDA criteria, indicating that an *IVIVR* could be product-specific and therefore, caution should be exercised when attempting to generalize results to different products containing the same active ingredient. It is likely that the considerable differences in the matrix designs used across commercial nitroglycerin TDS [29], with consequently different drug release profiles, could explain the failed *IVIVR* seen for the nitroglycerin TDS used here for external validation. For example, the application area of the Minitran® TDS is smaller than that of the other TDS examined, while this product is also unique in containing glyceryl monolaurate and ethyl oleate as penetration enhancers [29]. Other examples of product specific *IVIVC* or *IVIVR* for TDS exist, such as that reported for estradiol [72].

We suspect that the good *IVIVR* observed for nitroglycerin reflects a counterbalancing of its potential local vasodilatory promotion of *in vivo* skin absorption by a lower skin first pass metabolism in the *in vitro* skin. Skin has been reported to have a first pass loss of about 25% of that absorbed [73] and its esterase activity is impaired in frozen or heated separated skin [74]. The reason for the higher plasma levels predicted from *in vitro* studies compared to the observed data is unknown. There are a number of possible causes, including the use of different skin sites for *in vitro* and *in vivo* studies; increased *in vitro* skin permeability caused by damage to the skin barrier during collection, storage and preparation for Franz cell studies; alteration of skin permeability induced by interaction with the *IVPT* receptor phase, and promotion of solute solubility in that phase [75].

There are several limitations of the current work. First, there is the lack of data to enable an evaluation of the predictability of the derived *IVIVR*s. A low internal prediction error was found for the global pharmacokinetic parameters derived for nitroglycerin and rivastigmine. However, only the abdomen and upper arm data for rivastigmine would meet equivalent criteria to those specified by the US FDA for an *ER* product of an average percent prediction error (% PE) of 10% or less for C_{ss} and AUC_{last} to establish the predictability of the *IVIVC*. This finding, relative to the other rivastigmine sites, would justify the typical use of abdominal skin for *IVPT* studies. In principle, extension to other sites and impaired skin may be made by using morphological and SC function measures as discussed earlier, and as shown in Fig. 8. However, the extent to which this can be done robustly has yet to be validated. Furthermore, the current work is limited to those TDS products which have a relatively constant drug delivery rate over the entire period of application and are relatively stable and consistent because metamorphosis is minimal. More complicated models would be required to interpret the dynamic (metamorphic) complexities present in other dosage forms or delivery systems and to take into account excipient induced SC penetration enhancement. In addition, the model has assumed that transport through the skin has mainly been *via* diffusion in the SC and VE. As such, it does not account for the contribution of the appendageal skin delivery route [76,77] nor of facilitated transport as has been suggested to occur in the permeation of transfersomes [78],

with nanoemulsions [79] and with nanoparticles [80]. The model also assumes that absorption from the site is not affected by any clearance limitations from the skin into the body or of recirculating blood back to the absorption site from the systemic circulation. This is not strictly the case, for instance, with rivastigmine which displays some non-linearity in pharmacokinetics as a result of capacity limited elimination [30]. Last, but not least, the convolution approach we have used assumes there are no non-linearities in SC and VE transport processes, such as saturable binding or metabolism nor in plasma elimination kinetics. In these situations, an analytical solution may not be possible and a numerical approach offered by modifying and extending the compartment-in-series model would be rather more straightforward. The main limitation of this approach is that it uses a numerical compartment-in-series model that does not readily provide asymptotic solutions and is in a simplistic form, needing to be modified to account the earlier described appendageal and advanced delivery system transport mechanisms as well as skin heterogeneity and variations in barrier properties. Such an approach would also allow the reported non-linearity in rivastigmine pharmacokinetics as a result of capacity limited elimination [30] and the dose dependent pharmacokinetics of intravenous nitroglycerin infusions [81] to be better accommodated than was possible here. However, the approach presented here does provide analytical solutions as well as a numerical compartment-in-series approach which can be used to validate mechanistically more complex and accurate description of skin absorption as well as non-linearities in skin absorption and elimination.

5. Conclusions

In this work, we developed pharmacokinetic models in the Laplace domain to analyse *in vivo* plasma concentration-time profiles. Numerical inversion of the models described time-dependent skin permeation and gave an accurate estimation of steady-state skin permeation flux and diffusion time of compounds through the skin. The simple analytical solutions were resolved for later time points when skin permeation had reached steady state. We used the findings to establish *IVIVRs* for nitroglycerin and rivastigmine TDS based on their human skin *IVPT* results.

The pharmacokinetic models evaluated here serve as a basis of reference for further development of more sophisticated pharmacokinetic models. The ideal model would be able to interpret the dynamic (metamorphic) complexities of semisolid dosage forms, including physiologically-based PK (PBPK) models that can account for the variation in the permeability of the skin among different anatomical sites in an individual, and among different individuals in the population.

Acknowledgements

This research was carried out at the Translational Research Institute, Woolloongabba, QLD 4102, Australia. The Translational Research Institute is supported by a grant from the Australian Government. Funding for this project was also made possible, in part, by the U.S. Food and Drug Administration through grant U01FD005232 and by grants from the National Health and Medical Research Council of Australia (APP1049906; 1002611). Views expressed in this paper do not reflect official policies of the Department of Health and Human Services; nor does any mention of trade names, commercial practices, or organization imply endorsement by the United States Government.

References

[1] M.N. Pastore, Y.N. Kalia, M. Horstmann, M.S. Roberts, Transdermal patches: history, development and pharmacology, Br. J. Pharmacol. 172 (2015) 2179–2209.
[2] C. Herkenne, A. Naik, Y.N. Kalia, J. Hadgraft, R.H. Guy, Dermatopharmacokinetic prediction of topical drug bioavailability in vivo, J. Investig. Dermatol. 127 (2007) 887–894.
[3] C. Herkenne, A. Naik, Y.N. Kalia, J. Hadgraft, R.H. Guy, Ibuprofen transport into and through skin from topical formulations: in vitro-in vivo comparison, J. Investig. Dermatol. 127 (2007) 135–142.
[4] S. Wiedersberg, A. Naik, C.S. Leopold, R.H. Guy, Pharmacodynamics and dermatopharmacokinetics of betamethasone 17-valerate: assessment of topical bioavailability, Br. J. Dermatol. 160 (2009) 676–686.
[5] S.E. Cross, C. Anderson, M.S. Roberts, Topical penetration of commercial salicylate esters and salts using human isolated skin and clinical microdialysis studies, Br. J. Clin. Pharmacol. 46 (1998) 29–35.
[6] M. Bodenlenz, C. Hofferer, C. Magnes, R. Schaller-Ammann, L. Schaupp, F. Feichtner, M. Ratzer, K. Pickl, F. Sinner, A. Wutte, S. Korsatko, G. Kohler, F. J. Legat, E.M. Benfeldt, A.M. Wright, D. Neddermann, T. Jung, T.R. Pieber, Dermal PK/PD of a lipophilic topical drug in psoriatic patients by continuous intradermal membrane-free sampling, Eur. J. Pharm. Biopharm. 81 (2012) 635–641.
[7] M. Nivsarkar, S.H. Maroo, K.R. Patel, D.D. Patel, Evaluation of skin penetration of Diclofenac from a novel topical non aqueous solution: a comparative bioavailability study, J. Clin. Diagn. Res. 9 (2015) FC11–13.
[8] R.L. Bronaugh, R.C. Wester, D. Bucks, H.I. Maibach, R. Sarason, In vivo percutaneous absorption of fragrance ingredients in rhesus monkeys and humans, Food Chem. Toxicol. 28 (1990) 369–373.
[9] D.A. Bucks, H.I. Maibach, R.H. Guy, Percutaneous absorption of steroids: effect of repeated application, J. Pharm. Sci. 74 (1985) 1337–1339.
[10] D.A. Bucks, J.R. McMaster, H.I. Maibach, R.H. Guy, Percutaneous absorption of phenols in vivo, Clin. Res. 35 (1987) 672A.
[11] R.J. Feldmann, H.I. Maibach, Penetration of 14c hydrocortisone through Normal skin: the effect of stripping and occlusion, Arch. Dermatol. 91 (1965) 661–666.
[12] H.I. Maibach, R.J. Feldmann, Systemic Absorption of Pesticides through the Skin of Man, in: Occupational Exposure to Pesticides. Report to the Federal Working Group on Occupational Exposure to Pesticides, US Government Printing Office, Washington, DC, 1975, pp. 120–127.
[13] Y.G. Anissimov, M.S. Roberts, Diffusion modeling of percutaneous absorption kinetics. 1. Effects of flow rate, receptor sampling rate, and viable epidermal resistance for a constant donor concentration, J. Pharm. Sci. 88 (1999) 1201–1209.
[14] Y.G. Anissimov, M.S. Roberts, Diffusion modeling of percutaneous absorption kinetics: 2. Finite vehicle volume and solvent deposited solids, J. Pharm. Sci. 90 (2001) 504–520.
[15] Y.G. Anissimov, M.S. Roberts, Diffusion modeling of percutaneous absorption kinetics: 3. Variable diffusion and partition coefficients, consequences for stratum corneum depth profiles and desorption kinetics, J. Pharm. Sci. 93 (2004) 470–487.
[16] Y.G. Anissimov, M.S. Roberts, Diffusion modelling of percutaneous absorption kinetics: 4. Effects of a slow equilibration process within stratum corneum on absorption and desorption kinetics, J. Pharm. Sci. 98 (2009) 772–781.
[17] H. Bando, M. Sahashi, T. Takagi, F. Yamashita, Y. Takakura, M. Hashida, Analysis of in vitro skin penetration of acyclovir prodrugs based on a diffusion model with a metabolic process, Int. J. Pharm. 135 (1996) 91–102.
[18] E.R. Cooper, Pharmacokinetics of skin penetration, J. Pharm. Sci. 65 (1976) 1396–1397.
[19] H.F. Frasch, A.M. Barbero, Application of numerical methods for diffusion-based modeling of skin permeation, Adv. Drug Deliv. Rev. 65 (2013) 208–220.
[20] H.F. Frasch, A.L. Bunge, The transient dermal exposure II: post-exposure absorption and evaporation of volatile compounds, J. Pharm. Sci. 104 (2015) 1499–1507.
[21] R.H. Guy, J. Hadgraft, A theoretical description relating skin penetration to the thickness of the applied medicament, Int. J. Pharm. 6 (1980) 321–332.
[22] J.M. Nitsche, T.F. Wang, G.B. Kasting, A two-phase analysis of solute partitioning into the stratum corneum, J. Pharm. Sci. 95 (2006) 649–666.
[23] T.F. Wang, G.B. Kasting, J.M. Nitsche, A multiphase microscopic diffusion model for stratum corneum permeability. I. Formulation, solution, and illustrative results for representative compounds, J. Pharm. Sci. 95 (2006) 620–648.
[24] F. Yu, G.B. Kasting, A geometrical model for diffusion of hydrophilic compounds in human stratum corneum, Math. Biosci. 300 (2018) 55–63.
[25] K.D. McCarley, A.L. Bunge, Physiologically relevant one-compartment pharmacokinetic models for skin. 1. Development of models, J. Pharm. Sci. 87 (1998) 470–481.
[26] K.D. McCarley, A.L. Bunge, Physiologically relevant two-compartment pharmacokinetic models for skin, J. Pharm. Sci. 89 (2000) 1212–1235.
[27] A.A. Amarah, D.G. Petlin, J.E. Grice, J. Hadgraft, M.S. Roberts, Y.G. Anissimov, Compartmental modeling of skin transport, Eur. J. Pharm. Biopharm. 130 (2018) 336–344.
[28] R.L. Cleek, A.L. Bunge, A new method for estimating dermal absorption from chemical exposure. 1. General approach, Pharm. Res. 10 (1993) 497–506.
[29] J. Hadgraft, D. Lewis, D. Beutner, H.M. Wolff, In vitro assessments of transdermal devices containing nitroglycerin, Int. J. Pharm. 73 (1991) 125–130.
[30] U.S. Department of Health and Human Services, Food and Drug Administration, Center for Drug Evaluation and Research (CDER): Clinical Pharmacology and Biopharmaceutics Review (Rivastigmine) (Application Number 22–083), 2007, p. 43, http://www.accessdata.fda.gov/drugsatfda_docs/nda/2007/022083s000_ClinPharmR_P1.pdf (Accessed on: 30/04/2020).
[31] P.K. Noonan, M.A. Gonzalez, D. Ruggirello, J. Tomlinson, E. Babcock-Atkinson, M. Ray, A. Golub, A. Cohen, Relative bioavailability of a new transdermal nitroglycerin delivery system, J. Pharm. Sci. 75 (1986) 688–691.
[32] M. Hossain, S.S. Jhee, T. Shiovitz, C. McDonald, G. Sedek, F. Pommier, N.R. Cutler, Estimation of the absolute bioavailability of rivastigmine in patients with mild to moderate dementia of the Alzheimer's type, Clin. Pharmacokinet. 41 (2002) 225–234.

[33] E.F. McNiff, A. Yacobi, F.M. Young-Chang, L.H. Golden, A. Goldfarb, H.L. Fung, Nitroglycerin pharmacokinetics after intravenous infusion in normal subjects, J. Pharm. Sci. 70 (1981) 1054–1058.

[34] D.Z. D'Argenio, A. Schumitzky, X. Wang, ADAPT 5 User's Guide: Pharmacokinetic/Pharmacodynamic Systems Analysis Software, Biomedical Simulations Resource, Los Angeles, 2009.

[35] J.G. Wagner, E. Nelson, Kinetic analysis of blood levels and urinary excretion in the absorptive phase after single doses of drug, J. Pharm. Sci. 53 (1964) 1392–1403.

[36] J. Hadgraft, Pharmaceutical aspects of transdermal nitroglycerin, Int. J. Pharm. 135 (1996) 1–11.

[37] U.S. Department of Health and Human Services, Food and Drug Administration, Center for Drug Evaluation and Research (CDER): Guidance for Industry. Extended Release Oral Dosage Forms: Development, Evaluation, and Application of In Vitro/In Vivo Correlations. https://www.fda.gov/downloads/drugs/guidances/ucm070239.pdf, 1997 (Accessed on: 30/04/2020).

[38] W. Cawello, M. Braun, J.O. Andreas, Drug delivery and transport into the central circulation: an example of zero-order in vivo absorption of Rotigotine from a transdermal patch formulation, Eur. J. Drug Metab. Pharmacokinet. 43 (2018) 475–481.

[39] M. Mallandrich, F. Fernandez-Campos, B. Clares, L. Halbaut, C. Alonso, L. Coderch, M.L. Garduno-Ramirez, B. Andrade, A. Del Pozo, M.E. Lane, A.C. Calpena, Developing transdermal applications of ketorolac Tromethamine entrapped in stimuli sensitive block copolymer hydrogels, Pharm. Res. 34 (2017) 1728–1740.

[40] H. Olsson, R. Sandstrom, A. Neijber, D. Carrara, L. Grundemar, Pharmacokinetics and bioavailability of a new testosterone gel formulation in comparison to Testogel (R) in healthy men, Clin. Pharmacol. Drug Dev. 3 (2014) 358–364.

[41] R.J. Scheuplein, I.H. Blank, G.J. Brauner, D.J. MacFarlane, Percutaneous absorption of steroids, J. Invest. Dermatol. 52 (1969) 63–70.

[42] Y.G. Anissimov, M.S. Roberts, A compartmental model of hepatic disposition kinetics: 1. Model development and application to linear kinetics, J. Pharmacokinet. Pharmacodyn. 29 (2002) 131–156.

[43] K. Harada, T. Murakami, E. Kawasaki, Y. Higashi, S. Yamamoto, N. Yata, In-vitro permeability to salicylic acid of human, rodent, and shed snake skin, J. Pharm. Pharmacol. 45 (1993) 414–418.

[44] R.C. Scott, M.A. Corrigan, F. Smith, H. Mason, The influence of skin structure on permeability: an intersite and interspecies comparison with hydrophilic penetrants, J. Invest. Dermatol. 96 (1991) 921–925.

[45] M.S. Roberts, W.A. Favretto, A. Meyer, M. Reckmann, T. Wongseelashote, Topical bioavailability of methyl salicylate, Aust. NZ J. Med. 12 (1982) 303–305.

[46] A. Rougier, C. Lotte, H.I. Maibach, In vivo percutaneous penetration of some organic compounds related to anatomic site in humans: predictive assessment by the stripping method, J. Pharm. Sci. 76 (1987) 451–454.

[47] J.E. Shaw, M.E. Prevo, A.A. Amkraut, Testing of controlled-release transdermal dosage forms. Product development and clinical trials, Arch. Dermatol. 123 (1987) 1548–1556.

[48] L.S. Abrams, D.M. Skee, J. Natarajan, F.A. Wong, G.D. Anderson, Pharmacokinetics of a contraceptive patch (Evra/Ortho Evra) containing norelgestromin and ethinyloestradiol at four application sites, Br. J. Clin. Pharmacol. 53 (2002) 141–146.

[49] J. Hochel, B. Schuett, M. Ludwig, C. Zurth, Implications of different application sites on the bioavailability of a transdermal contraceptive patch containing ethinyl estradiol and gestodene: an open-label, randomized, crossover study, Int. J. Clin. Pharmacol. Ther. 52 (2014) 856–866.

[50] J.L. Bormann, H.I. Maibach, Effects of anatomical location on in vivo percutaneous penetration in man, Cutan. Ocul. Toxicol. 39 (2020) 213–222.

[51] U.S. Department of Health and Human Services, Food and Drug Administration, Center for Drug Evaluation and Research (CDER): Clinical Pharmacology and Biopharmaceutics Review (Asenapine) (Application Number 212268Orig1s000), 2018, pp. 64–65, https://www.accessdata.fda.gov/drugsatfda_docs/nda/2019/212268Orig1s000MultidisciplineR.pdf (Accessed on: 26/03/2021).

[52] U.S. Department of Health and Human Services, Food and Drug Administration, Center for Drug Evaluation and Research (CDER): Clinical Pharmacology and Biopharmaceutics Review (Buprenorphine), (Application Number 21–306), pp. 43 (2010), https://www.accessdata.fda.gov/drugsatfda_docs/nda/2010/021306Orig1s000ClinPharmR.pdf Accessed on: 26/03/2021.

[53] A. Ebihara, A. Fujimura, K. Ohashi, T. Shiga, Y. Kumagai, H. Nakashima, T. Kotegawa, Influence of application site of a new transdermal clonidine, M-5041T, on its pharmacokinetics and pharmacodynamics in healthy subjects, J. Clin. Pharmacol. 33 (1993) 1188–1191.

[54] U.S. Department of Health and Human Services, Food and Drug Administration, Center for Drug Evaluation and Research (CDER): Clinical Pharmacology and Biopharmaceutics Review (Fentanyl), (Application Number 19–813/S044), pp. 235–236 (2009), https://www.accessdata.fda.gov/drugsatfda_docs/nda/2009/019813Orig1s044.pdf Accessed on: 26/03/2021.

[55] S. Sobue, K. Sekiguchi, H. Kikkawa, S. Irie, Effect of application sites and multiple doses on nicotine pharmacokinetics in healthy male Japanese smokers following application of the transdermal nicotine patch, J. Clin. Pharmacol. 45 (2005) 1391–1399.

[56] J.-P. Elshoff, M. Braun, J.-O. Andreas, M. Middle, W. Cawello, Steady-state plasma concentration profile of transdermal rotigotine: an integrated analysis of three, open-label, randomized, phase I multiple dose studies, Clin. Ther. 34 (2012) 966–978.

[57] Z. Yu, S.K. Gupta, S.S. Hwang, D.M. Cook, M.J. Duckett, L.E. Atkinson, Transdermal testosterone administration in hypogonadal men: comparison of pharmacokinetics at different sites of application and at the first and fifth days of application, J. Clin. Pharmacol. 37 (1997) 1129–1138.

[58] A. Rougier, D. Dupuis, C. Lotte, R. Roguet, R.C. Wester, H.I. Maibach, Regional variation in percutaneous absorption in man: measurement by the stripping method, Arch. Dermatol. Res. = Archiv. Dermatol. Forschung 278 (1986) 465–469.

[59] C. Lotte, A. Rougier, D.R. Wilson, H.I. Maibach, In vivo relationship between transepidermal water loss and percutaneous penetration of some organic compounds in man: effect of anatomic site, Arch. Dermatol. Res. = Archiv. Dermatol. Forsch. 279 (1987) 351–356.

[60] A.K. Shah, G. Wei, R.C. Lanman, V.O. Bhargava, S.J. Weir, Percutaneous absorption of ketoprofen from different anatomical sites in man, Pharm. Res. 13 (1996) 168–172.

[61] R.J. Feldmann, H.I. Maibach, Regional variation in percutaneous penetration of 14C cortisol in man, J. Invest. Dermatol. 48 (1967) 181–183.

[62] H.I. Maibach, R.J. Feldman, T.H. Milby, W.F. Serat, Regional variation in percutaneous penetration in man, Pesticides Arch. Environ. Health 23 (1971) 208–211.

[63] S. Polak, C. Ghobadi, H. Mishra, M. Ahamadi, N. Patel, M. Jamei, A. Rostami-Hodjegan, Prediction of concentration-time profile and its inter-individual variability following the dermal drug absorption, J. Pharm. Sci. 101 (2012) 2584–2595.

[64] A. Bohling, S. Bielfeldt, A. Himmelmann, M. Keskin, K.P. Wilhelm, Comparison of the stratum corneum thickness measured in vivo with confocal Raman spectroscopy and confocal reflectance microscopy, Skin Res. Technol. 20 (2014) 50–57.

[65] Z. Ya-Xian, T. Suetake, H. Tagami, Number of cell layers of the stratum corneum in normal skin - relationship to the anatomical location on the body, age, sex and physical parameters, Arch. Dermatol. Res. = Archiv. Dermatol. Forsch. 291 (1999) 555–559.

[66] K. Biniek, J. Kaczvinsky, P. Matts, R.H. Dauskardt, Understanding age-induced alterations to the biomechanical barrier function of human stratum corneum, J. Dermatol. Sci. 80 (2015) 94–101.

[67] D. Bucks, Permeability through diseased and damaged skin, in: K.A. Walters, M. S. Roberts (Eds.), Dermatologic, Cosmeceutic, and Cosmetic Development: Therapeutic and Novel Approaches, Informa Healthcare, Boca Raton, 2008, pp. 157–167.

[68] V. Purohit, S. Riley, H. Tan, W.C. Ports, Predictors of systemic exposure to topical Crisaborole: a nonlinear regression analysis, J. Clin. Pharmacol. 60 (2020) 1344–1354.

[69] T. Montero-Vilchez, M.V. Segura-Fernandez-Nogueras, I. Perez-Rodriguez, M. Soler-Gongora, A. Martinez-Lopez, A. Fernandez-Gonzalez, A. Molina-Leyva, S. Arias-Santiago, Skin barrier function in psoriasis and atopic dermatitis: transepidermal water loss and temperature as useful tools to assess disease severity, J. Clin. Med. 10 (2021).

[70] H. Zainal, A. Jamil, N. Md Nor, M.M. Tang, Skin pH mapping and its relationship with transepidermal water loss, hydration and disease severity in adult patients with atopic dermatitis, Skin Res. Technol. 26 (2020) 91–98.

[71] P.A. Lehman, S.G. Raney, T.J. Franz, Percutaneous absorption in man: in vitro-in vivo correlation, Skin Pharmacol. Physiol. 24 (2011) 224–230.

[72] Y. Yang, P. Manda, N. Pavurala, M.A. Khan, Y.S. Krishnaiah, Development and validation of in vitro-in vivo correlation (IVIVC) for estradiol transdermal drug delivery systems, J. Control. Release 210 (2015) 58–66.

[73] E. Nakashima, P.K. Noonan, L.Z. Benet, Transdermal bioavailability and first-pass skin metabolism: a preliminary evaluation with nitroglycerin, J. Pharmacokinet. Biopharm. 15 (1987) 423–437.

[74] W.M. Lau, K.W. Ng, K. Sakenyte, C.M. Heard, Distribution of esterase activity in porcine ear skin, and the effects of freezing and heat separation, Int. J. Pharm. 433 (2012) 10–15.

[75] S. Yousef, X. Liu, A. Mostafa, Y. Mohammed, J.E. Grice, Y.G. Anissimov, W. Sakran, M.S. Roberts, Estimating maximal in vitro skin permeation flux from studies using non-sink receptor phase conditions, Pharm. Res. 33 (2016) 2180–2194.

[76] X. Liu, J.E. Grice, J. Lademann, N. Otberg, S. Trauer, A. Patzelt, M.S. Roberts, Hair follicles contribute significantly to penetration through human skin only at times soon after application as a solvent deposited solid in man, Br. J. Clin. Pharmacol. 72 (2011) 768–774.

[77] E. Abd, H.A.E. Benson, M.S. Roberts, J.E. Grice, Minoxidil skin delivery from Nanoemulsion formulations containing eucalyptol or oleic acid: enhanced diffusivity and follicular targeting, Pharmaceutics 10 (2018) 19.

[78] R. Rajan, S. Jose, V.P. Mukund, D.T. Vasudevan, Transferosomes - a vesicular transdermal delivery system for enhanced drug permeation, J. Adv. Pharm. Technol. Res. 2 (2011) 138–143.

[79] E. Abd, S. Namjoshi, Y.H. Mohammed, M.S. Roberts, J.E. Grice, Synergistic skin penetration enhancer and Nanoemulsion formulations promote the human epidermal permeation of caffeine and naproxen, J. Pharm. Sci. 105 (2016) 212–220.

[80] P. Ghasemiyeh, S. Mohammadi-Samani, Potential of nanoparticles as permeation enhancers and targeted delivery options for skin: advantages and disadvantages, Drug Des. Devel. Ther. 14 (2020) 3271–3289.

[81] P.K. Noonan, R.L. Williams, L.Z. Benet, Dose dependent pharmacokinetics of nitroglycerin after multiple intravenous infusions in healthy volunteers, J. Pharmacokinet. Biopharm. 13 (1985) 143–157.